

SECOND-ORDER RAYLEIGH–SCHRÖDINGER PERTURBATION THEORY FOR THE GRASP2018 PACKAGE: THREE-PARTICLE FEYNMAN DIAGRAM CONTRIBUTION TO VALENCE–VALENCE CORRELATIONS*

G. Gaigalas, P. Rynkun, and L. Kitovienė

Institute of Theoretical Physics and Astronomy, Faculty of Physics, Vilnius University, Saulėtekio 3, 10257 Vilnius, Lithuania

Email: gediminas.gaigalas@tfai.vu.lt; pavel.rynkun@tfai.vu.lt; laima.radziute@tfai.vu.lt

Received 3 June 2025; revised 16 June 2025; accepted 18 June 2025

The method based on the second-order perturbation theory to identify the most important configuration state functions of various correlations is extended to include valence–valence correlations, which are described by the three-particle Feynman diagram. The extension presented in this work complements the core–valence, core, core–core and valence–valence correlations which were developed in a series of previous papers by G. Gaigalas, P. Rynkun, and L. Kitovienė. Whereas these valence–valence correlations are described by the three-particle Feynman diagram, additional developments to calculate the spin-angular parts of this diagram have been made to the program library **librang** of the GRASP. As an example of the application of the developed method, the atomic calculations of the energy structure for the Se III ion are presented. In the present work, this method was also used to select the most significant configuration state functions and to use this basis to solve the self-consistent field equations.

Keywords: configuration interaction, spin-angular integration, perturbation theory, tensorial algebra, valence–valence correlations, core–valence correlations, core correlations, core–core correlations

1. Introduction

An approach based on a combination of the relativistic configuration interaction method and the stationary second-order Rayleigh–Schrödinger many-body perturbation theory (RSMBPT) in an irreducible tensorial form has recently been developed [1–4]. It allows us to analyze effectively core–valence (CV), core (C), core–core (CC) and valence–valence (VV) correlations using the General Relativistic Atomic Structure Package GRASP [5], which are described by vacuum, one- and two-particle Feynman diagrams. At the same time, this theory extends the potential of the methodology [6, 7] used worldwide.

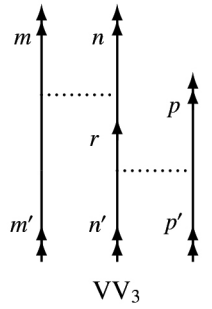
The formulation of this theory is based on the second-order linked-diagram theorem (Ref. [8], Section 12.5.2), where the lines of the Feynman diagrams corresponding to the electronic excitations are linked together to form a solid line. Based on this theorem, we further develop the capabilities

of the theory in this paper. For completeness, we include in the paper (Section 2) the three-particle Feynman diagram describing the valence–valence correlations. Since the spin-angular part of this diagram is much more complex, a major part of the paper is devoted to the calculation of the spin-angular coefficients (Section 3). The final expressions are presented in Section 4 of the paper. Section 5 contains the calculations showing that the expressions and the examination of valence–valence correlations presented in the paper are correct and usable. The conclusions are presented in Section 6.

2. Relativistic second-order effective Hamiltonian of an atom or ion in an irreducible tensorial form for the remaining valence–valence correlations

New Feynman diagrams are used to describe valence–valence correlations, which were not available for core–valence, core and core–core correlations. We discuss this in detail below.

* Dedicated to the memory of professor **Zenonas Rokus Rudzikas** (1940–2011) on the occasion of his birth anniversary.



$$\begin{aligned}
 &= - \sum_{m,m'} \sum_{n,n'} \sum_{p,p'} \sum_{k,k',x} (-1)^{j_n+j_{n'}+k+k'} \sqrt{\frac{[x]}{[k,k']}} \\
 &\times \left[\left[a^{(j_m)} \times \tilde{a}^{(j_{m'})} \right]^{(k)} \times \left[a^{(j_n)} \times \tilde{a}^{(j_{n'})} \right]^{(x)} \times \left[a^{(j_p)} \times \tilde{a}^{(j_{p'})} \right]^{(k')} \right]^{(0)} \\
 &\times \sum_r \frac{1}{(\varepsilon_{n'} + \varepsilon_{p'} - \varepsilon_r - \varepsilon_p)} \left\{ \begin{matrix} j_{n'} & j_n & x \\ k & k' & j_r \end{matrix} \right\} X_k(mn, m'r) X_{k'}(rp, n'p')
 \end{aligned}$$

Fig. 1. The VV Feynman diagram of the second-order effective Hamiltonian for the third and fourth types of valence–valence correlations $(n_m \ell_m) j_m^{w_m} (n_n \ell_n) j_n^{w_n} \rightarrow (n_m \ell_m) j_m^{w_{m+1}} (n_n \ell_n) j_n^{w_{n-2}} (n_r \ell_r) j_r$ and $(n_m \ell_m) j_m^{w_m} (n_n \ell_n) j_n^{w_n} (n_p \ell_p) j_p^{w_p} \rightarrow (n_m \ell_m) j_m^{w_{m+1}} (n_n \ell_n) j_n^{w_{n-1}} (n_p \ell_p) j_p^{w_{p-1}} (n_r \ell_r) j_r$.

2.1. The third type of valence–valence correlations

The first two types of valence–valence correlations are already described in the paper [4]. The third type of valence–valence correlations is presented through the Feynman diagram VV_3 from Fig. 1, where all lines with the double arrow of diagram are renamed in the following way: $m' = p \equiv m$ and $m = n = n' = p' \equiv n$.

$$\begin{aligned}
 &(n_m \ell_m) j_m^{w_m} (n_n \ell_n) j_n^{w_n} \rightarrow \\
 &\rightarrow (n_m \ell_m) j_m^{w_{m+1}} (n_n \ell_n) j_n^{w_{n-2}} (n_r \ell_r) j_r.
 \end{aligned} \quad (1)$$

The expression of the three-particle Feynman diagram VV_3 , like the diagrams described in the previous papers [1–4], have the energy denominator $D = \Sigma(\varepsilon_{\text{down}} - \varepsilon_{\text{up}})$, where $\varepsilon_{\text{down}}$ (ε_{up}) is the single-particle eigenvalue associated with the down- (up-)orbital lines to (from) the lowest interaction line of the diagram. For example, the denominators for the VV_3 diagram are

$$D = (\varepsilon_{n'} + \varepsilon_{p'} - \varepsilon_r - \varepsilon_p), \quad (2)$$

where the indexes n' , p' and p belong to the F' set, and r belongs to the G set of orbitals [1].

Also, the following notations are used in the expressions of this diagram (see Fig. 1):

$$\begin{aligned}
 X_k(ij, i'j') &= \langle \ell_i j_i || C^{(k)} || \ell_{i'} j_{i'} \rangle \langle \ell_j j_j || C^{(k)} || \ell_{j'} j_{j'} \rangle \times \\
 &\times R^k(n_i j_i n_j j_j, n_{i'} j_{i'} n_{j'} j_{j'}),
 \end{aligned} \quad (3)$$

where $R^k(n_i j_i n_j j_j, n_{i'} j_{i'} n_{j'} j_{j'})$ is the radial integral of the electrostatic interaction between electrons

(Ref. [6], Eqs. (89) and (90)) and $\langle \ell_i j_i || C^{(k)} || \ell_{i'} j_{i'} \rangle$ is the reduced matrix element of the irreducible tensor operator $C^{(k)}$ in the jj -coupling.

In contrast to the previous diagrams (see Refs. [1–4]), this diagram has six operators of the second quantization (three pairs of creation and annihilation operators). This complicates finding the values of the spin-angular coefficient of this diagram and therefore makes the program library `librang` [9] from GRASP unusable in the most general case. This problem will be discussed and solved in detail in the next section.

2.2. The fourth type of valence–valence correlations

The following type of the correlation

$$\begin{aligned}
 &(n_m \ell_m) j_m^{w_m} (n_n \ell_n) j_n^{w_n} (n_p \ell_p) j_p^{w_p} \rightarrow \\
 &\rightarrow (n_m \ell_m) j_m^{w_{m+1}} (n_n \ell_n) j_n^{w_{n-1}} (n_p \ell_p) j_p^{w_{p-1}} (n_r \ell_r) j_r
 \end{aligned} \quad (4)$$

is described by the same diagram VV_3 with four different sets of open lines with double-arrow indices. Four diagrams A_1 , A_2 , A_3 and A_4 from Fig. 2 represent all these different sets. For example, the Feynman diagram A_1 has the following values: $m = p' \equiv n$, $m' = p \equiv m$ and $n = n' \equiv p$. Therefore, to find the value of this type of correlation, it is necessary to analyze all four diagrams: A_1 , A_2 , A_3 and A_4 . But it is easy to see that these diagrams can be converted into a search for two diagrams A_5 ($A_5 \equiv A_1$) and A_6 ($A_6 \equiv A_3$) with a multiplier $(1 + P(\dots))$, where the notation $P(n \rightleftharpoons p)$ means that the diagrams need a substitution of n to p and p to n . This makes it considerably easier to carry out the desired calculations. Note that A_5 describes the direct part of the correlation under

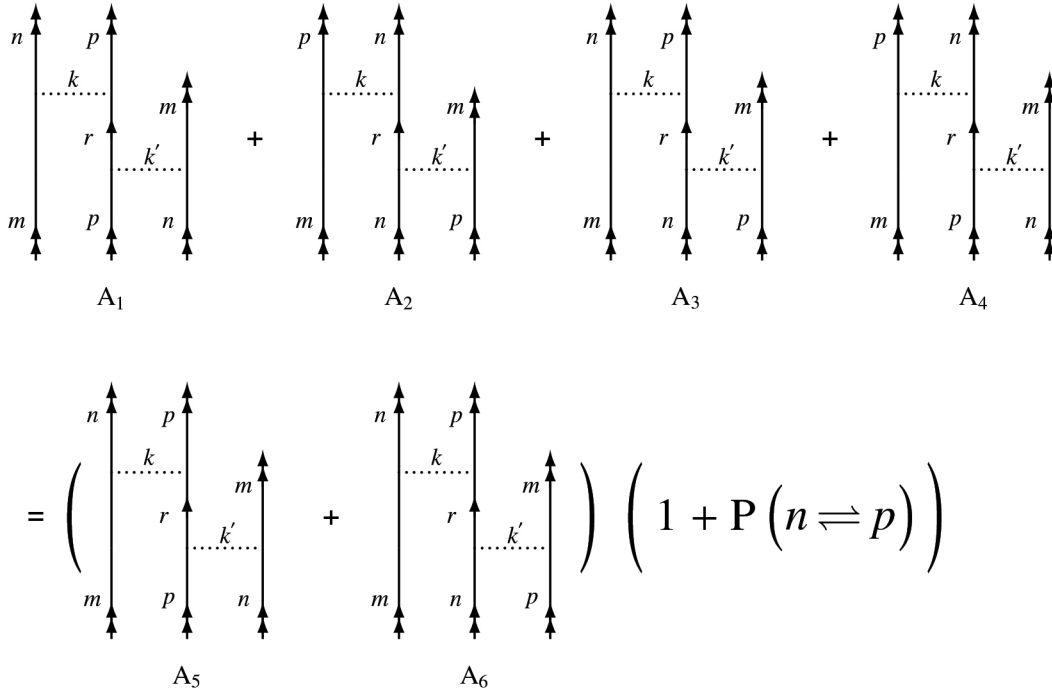


Fig. 2. The VV Feynman diagrams of the second-order effective Hamiltonian, expressing the fourth type of valence–valence correlations $(n_m \ell_m) j_m^{w_m} (n_n \ell_n) j_n^{w_n} (n_p \ell_p) j_p^{w_p} \rightarrow (n_m \ell_m) j_m^{w_m+1} (n_n \ell_n) j_n^{w_n-1} (n_p \ell_p) j_p^{w_p-1} (n_r \ell_r) j_r$.

consideration, while A_6 describes the exchange part of the interaction. These A_5 and A_6 are the three-particle Feynman diagram for which the program library `librang` [9] from GRASP does not support the calculation of spin-angular parts. It is, therefore, necessary to extend the capabilities of this program library to calculate the values of these diagrams. This problem will be discussed and solved in detail in the next section.

3. The spin-angular part of the three-particle Feynman diagram contributing to valence–valence correlations

The program library `librang` [9] from GRASP evaluates spin-angular coefficients of any matrix element with any number of open subshells for any one- and/or two-particle operators. Therefore, in previous papers [1–4], when developing the combination of the second-order Rayleigh–Schrödinger perturbation theory and the relativistic configuration interaction method, there was no problem in using it to find correlations described by vacuum, one- and two-particle Feynman diagrams. However, problems with using this library arise when dealing with three-particle operators.

The program library `librang` [9] is based on the spin-angular approach [10, 11]. The specifics of this approach (factorization of standard values, interaction strengths and recoupling matrices) makes it easy enough to extend it to allow the program library to find the spin-angular part of the VV_3 Feynman diagram that is needed to find the correlations that are being studied in this paper. This can be done by using ideas published in the paper [12], where the second quantization operators are grouped according to their action on the subshell, i.e. so that the second quantization operators act on the subshell m first, then on the subshell p (if there are any), and finally on the subshell n . Below, we show how this has been done for the different types of correlations, separately.

3.1. The spin-angular part of the third type of valence–valence correlations

In this case, the diagram VV_3 has the tensorial structure

$$\begin{aligned} & [[a_1^{(j_n)} \times \tilde{a}_2^{(j_m)}]^{(k)} \times [a_3^{(j_n)} \times \tilde{a}_4^{(j_n)}]^{(s)}]^{(k')} \times \\ & \times [a_5^{(j_m)} \times \tilde{a}_6^{(j_n)}]^{(k')}]^{(0)}, \end{aligned} \quad (5)$$

where the subscript next to the operator indicates the sequence number of the second quantization operator in the tensorial product. As seen in the tensorial structure (5), two pairs of second quantization operators are mixed, i.e. they consist of second quantization operators acting on different subshells. This is a pair consisting of operators with sequence numbers 1 and 2 and a pair with sequence numbers 5 and 6. This situation greatly complicates the study of the spin-angular part of this operator. But if we replace the tensorial structure (5) with the

$$\begin{aligned} & \left[[\tilde{a}_2^{(j_m)} \times a_5^{(j_m)}]^{(J_1)} \times \right. \\ & \left. \times [\tilde{a}_3^{(j_n)} \times \tilde{a}_4^{(j_n)}]^{(x)} \times [a_1^{(j_n)} \times \tilde{a}_6^{(j_n)}]^{(J_2)} \right]^{(J_1)} \right]^{(0)}, \quad (6) \end{aligned}$$

then the situation would change and one could easily extend the spin-angular approach [10, 11] to the study of the three-particle operator for this type of correlations [12]. This can be done by using the commutation rule of second quantization operators. This rule allows us to transform the tensorial product (5) into (6) using commutations, resulting in a suitable form for the calculation, in which we have a linear combination of two sets of tensorial operators. The first tensorial product $[\tilde{a}_2^{(j_m)} \times a_5^{(j_m)}]^{(J_1)}$ is the one to which we want to bring the algebraic expression, like in (6), and the second one $[[a_3^{(j_n)} \times \tilde{a}_4^{(j_n)}]^{(x)} \times [a_1^{(j_n)} \times \tilde{a}_6^{(j_n)}]^{(J_2)}]^{(J_1)}$ consists of only two pairs of operators for the second quantization acting to the same subshell. These two sets of tensorial operators are obtained by applying the operator commutation rule to operators $a_1^{(j_n)}$ and $\tilde{a}_4^{(j_n)}$. This gives the following expression:

$$\begin{aligned} & \left[[a^{(j_n)} \times \tilde{a}^{(j_m)}]^{(k)} \times [a^{(j_n)} \times \tilde{a}^{(j_n)}]^{(x)} \right]^{(k')} \times \\ & \times [a^{(j_m)} \times \tilde{a}^{(j_n)}]^{(k')} \right]^{(0)} = \sum_J B_1 [\tilde{a}^{(j_m)} \times a^{(j_m)}]^{(J)} \times \\ & [a^{(j_n)} \times \tilde{a}^{(j_n)}]^{(J)} \right]^{(0)} + \sum_{J_1, J_2} B_2 [\tilde{a}^{(j_m)} \times a^{(j_m)}]^{(J_1)} \times \\ & \times [a^{(j_n)} \times \tilde{a}^{(j_n)}]^{(J_2)} \right]^{(J_1)} \right]^{(0)}. \quad (7) \end{aligned}$$

The coefficients B_1 and B_2 in Eq. (7) are the easiest ones to represent and their algebraic expressions are the easiest coefficients to obtain by using the generalized graphical method

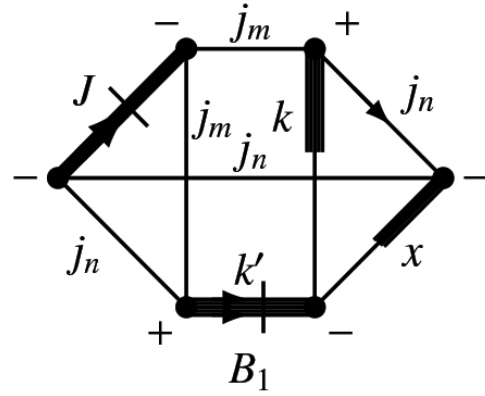


Fig. 3. Diagram showing the recoupling coefficient B_1 .

of the angular momentum theory [13]. In this graphical representation, the B_1 multiplier is shown graphically in Fig. 3, and the B_2 multiplier in Fig. 4.

Using the diagrams separation on the three lines theorem of Jucys, Levinson, and Vanagas (see Ref. [8], Section 4.1.3), it is possible to split the diagram B_1 into two diagrams, each representing a $6j$ -symbol [13, 14]. This rule is general and is used in all versions of the graphical methods for the angular momentum, whether the graphical method is applied to the Wigner coefficients [8, 15–18] or to the Clebsch–Gordan coefficients [13, 14, 17]. In this case, the diagram B_1 cuts through the horizontal lines j_m, j_n and k' . Meanwhile, the diagram B_2 uses a graphical technique [13, 14] to represent the $9j$ -symbol with additional multipliers. Eq. (7) can be rewritten as

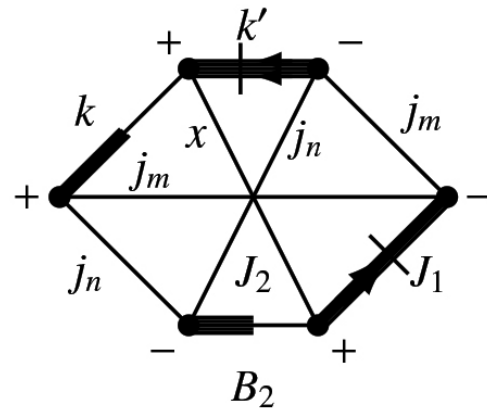


Fig. 4. Diagram showing the recoupling coefficient B_2 of the tensorial product from Eq. (5) to Eq. (6).

$$\begin{aligned}
& \left[\left[a^{(j_n)} \times \tilde{a}^{(j_m)} \right]^{(k)} \times \left[a^{(j_n)} \times \tilde{a}^{(j_n)} \right]^{(x)} \right]^{(k')} \times \\
& \times \left[a^{(j_m)} \times \tilde{a}^{(j_n)} \right]^{(k')} \Big]^{(0)} = \\
& = (-1)^{j_m+j_n+k+x} \sqrt{[k, k', x]} \left\{ \begin{matrix} j_m & j_n & k \\ x & k' & j_n \end{matrix} \right\} \times \\
& \times \sum_J (-1)^J \sqrt{[J]} \left\{ \begin{matrix} j_m & j_m & J \\ j_n & j_n & k' \end{matrix} \right\} \times \\
& \times \left[\left[\tilde{a}^{(j_m)} \times a^{(j_m)} \right]^{(J)} \times \left[a^{(j_n)} \times \tilde{a}^{(j_n)} \right]^{(J)} \right]^{(0)} + \\
& + (-1)^{j_m+j_n+k+x} \sqrt{[k, k']} \times \\
& \times \sum_{J_1, J_2} \sqrt{[J_1, J_2]} \left\{ \begin{matrix} j_m & j_n & k \\ J_1 & J_2 & x \\ j_m & j_n & k' \end{matrix} \right\} \times \\
& \times \left[\left[\tilde{a}^{(j_m)} \times a^{(j_m)} \right]^{(J_1)} \times \right. \\
& \times \left. \left[\left[a^{(j_n)} \times \tilde{a}^{(j_n)} \right]^{(x)} \times \left[a^{(j_n)} \times \tilde{a}^{(j_n)} \right]^{(J_2)} \right]^{(J_1)} \right]^{(0)}. \tag{8}
\end{aligned}$$

The first term in Eq. (8) corresponds to the spin-angular part of the two-particle operators. The program library `librang` [9] is therefore sufficient for its calculation. The second term, with its three pairs of second quantization operators, corresponds to the three-particle operator (6). In this case, adding new features to the library is necessary, which we will now discuss.

A peculiarity of the methodology [11] is that in the expression there (Ref. [11], Eq. (11)) the recoupling matrix $R(\lambda_p, \lambda_j, \lambda'_p, \lambda'_j, \Lambda^{bra}, \Lambda^{ket}, \Gamma)$, the submatrix element $T(n_i \lambda_i, n_j \lambda_j, n'_i \lambda'_i, n'_j \lambda'_j, \Lambda^{bra}, \Lambda^{ket}, \Xi, \Gamma)$, the phase factor Δ and $\Theta'(n_i \lambda_i, n_j \lambda_j, n'_i \lambda'_i, n'_j \lambda'_j, \Xi)$, which is proportional to the radial part, are easily separated from each other and can be treated differently. This fact makes the methodology flexible and allows it to be easily extended to include new class/type operators, such as the three-particle operator (6) that we are considering. In particular, how the expression (Ref. [11], Eq. (11)) is implemented in the library is described in the paper [9]. Here, we will now discuss only those aspects of the tensorial product (6) of Feynman diagram A_5 that were not covered in the paper [9] and will show which subroutines from the program library `librang` should be used and which expressions should be added to it.

Since we can schematically rewrite the tensorial product (8) as the tensorial product of two operators $A^{(J_1)}(n_m j_m)$ and $B^{(J_1)}(n_n j_n)$ acting on different subshells

$$[A^{(J_1)}(n_m j_m) \times B^{(J_1)}(n_n j_n)]^{(0)}, \tag{9}$$

the algebraic expression of the recoupling matrix can be used from the paper [11] (Eq. (19) there) and can be computed by the subroutine `RECO2` (Ref. [9], Section 3.2.4). Therefore, the library's librang existing capabilities are entirely sufficient for calculating $R(\lambda_p, \lambda_j, \lambda'_p, \lambda'_j, \Lambda^{bra}, \Lambda^{ket}, \Gamma)$.

As far as the submatrix element $T(n_i \lambda_i, n_j \lambda_j, n'_i \lambda'_i, n'_j \lambda'_j, \Lambda^{bra}, \Lambda^{ket}, \Xi, \Gamma)$ is concerned, the situation is different. In this case, the tensorial product can be split into two parts, i.e.

$$A^{(J_1)}(n_m j_m) \equiv [\tilde{a}^{(j_m)} \times a^{(j_m)}]^{(J_1)} \tag{10}$$

and

$$B^{(J_1)}(n_n j_n) \equiv [[a^{(j_n)} \times \tilde{a}^{(j_n)}]^{(x)} \times [a^{(j_n)} \times \tilde{a}^{(j_n)}]^{(J_2)}]^{(J_1)}. \tag{11}$$

These two members should be considered separately (because they act on different subshells, and the binding of the ranks of the tensorial structure is already included in the recoupling matrix). Subroutine `WJ1` (Ref. [9], Section 3.3.3)) finds the matrix element of operator (10), while the library `librang` has no suitable subroutine for computing the matrix element of the operator (11). To find the latter requires the use of an expression such as

$$\begin{aligned}
& \langle (n_n \ell_n) j_n^w \alpha J \| [[a^{(j_n)} \times \tilde{a}^{(j_n)}]^{(x)} \times \\
& \times [a^{(j_n)} \times \tilde{a}^{(j_n)}]^{(J_2)}]^{(J_1)} \| (n_n \ell_n) j_n^w \alpha' J' \rangle = \\
& = (-1)^{J+J'+J_1} \sqrt{[J_1]} \sum_{\alpha'' J''} \left\{ \begin{matrix} x & J_2 & J_1 \\ J' & J & J'' \end{matrix} \right\} \times \\
& \times \langle (n_n \ell_n) j_n^w \alpha J \| [a^{(j_n)} \times \tilde{a}^{(j_n)}]^{(x)} \\
& \| (n_n \ell_n) j_n^w \alpha'' J'' \rangle \times \\
& \langle (n_n \ell_n) j_n^w \alpha'' J'' \| [a^{(j_n)} \times \tilde{a}^{(j_n)}]^{(J_2)} \\
& \| (n_n \ell_n) j_n^w \alpha' J' \rangle. \tag{12}
\end{aligned}$$

Therefore, the library `librang` must be extended by programming the expression (12).

The phase factor Δ , according to Ref. [11], is zero.

The $\Theta'(n_i \lambda_i, n_j \lambda_j, n'_i \lambda'_i, n'_j \lambda'_j, \Xi)$, which is proportional to the radial part, is found in a regular way as it was found in papers [1–4].

Note that the above describes how to calculate the reduced matrix elements of the Feynman diagram VV_3 in the general case for the third type of valence–valence correlations. But it is possible to extract the individual parts which are more straightforward to calculate, i.e. the coefficient $\Delta \mathcal{E}_0$ (does not depend on the term), $\Delta \mathcal{F}^k(n, n)$ and $\Delta \mathcal{F}^k(m, n)$ (regular spin-angular library `librang` can be used). The extraction of these expressions is the same as in the papers [1–4]. Therefore, only the reduced matrix element of part of Feynman diagrams A_5 with a tensorial product (6) is calculated from the general expression when the rank $k > 0$. The part, which is calculated from the general expression, will be denoted by $\Delta \tilde{\mathcal{R}}^{(k, k', x)}(mnn)$ in the future.

3.2. The spin-angular part of the fourth type of valence–valence correlations

Two different Feynman diagrams A_5 and A_6 from Fig. 2 describe this type of correlation. We will consider each separately as their spin-angular part differs significantly.

3.2.1. The direct part of the fourth type of valence–valence correlations

Now let us discuss the diagram A_5 , with a tensorial structure:

$$\begin{aligned} & [[a_1^{(j_n)} \times \tilde{a}_2^{(j_m)}]^{(k)} \times [a_3^{(j_p)} \times \tilde{a}_4^{(j_p)}]^{(x)}]^{(k')} \times \\ & \times [a_5^{(j_m)} \times \tilde{a}_6^{(j_n)}]^{(k')}]^{(0)}. \end{aligned} \quad (13)$$

As in Eq. (5), Eq. (13) is not appropriate to calculate the spin-angular part because there are two pairs of secondary quantization operators acting on different subshells, i.e. $[a_1^{(j_n)} \times \tilde{a}_2^{(j_m)}]^{(k)}$ and $[a_5^{(j_m)} \times \tilde{a}_6^{(j_n)}]^{(k)}$. Therefore, this tensorial product has to be transformed into the following, using the commutation rules of the secondary quantization:

$$\begin{aligned} & [[\tilde{a}_2^{(j_m)} \times a_5^{(j_m)}]^{(j_1)} \times [a_3^{(j_p)} \times \tilde{a}_4^{(j_p)}]^{(x)}]^{(j_2)} \times \\ & \times [a_1^{(j_n)} \times \tilde{a}_6^{(j_n)}]^{(j_2)}]^{(0)}. \end{aligned} \quad (14)$$

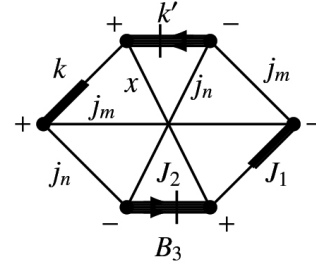


Fig. 5. Diagram showing the recoupling coefficient B_3 of the tensorial product from Eq. (13) to Eq. (14).

In this case, the transformation of the tensorial product from Eq. (13) to Eq. (14) results in only one member in Eq. (14), where the transformation matrix of the tensorial structure is shown graphically in Fig. 5. B_3 is proportional to the coefficient 9j-symbol [13, 14]. The final expression of this rearrangement of the tensorial structure (13) is the following:

$$\begin{aligned} & \left[\left[[a^{(j_n)} \times \tilde{a}^{(j_m)}]^{(k)} \times [a^{(j_p)} \times \tilde{a}^{(j_p)}]^{(x)} \right]^{(k')} \times \right. \\ & \left. \times [a^{(j_m)} \times \tilde{a}^{(j_n)}]^{(k')} \right]^{(0)} = \\ & = \sum_{J_1, J_2} B_3 \left[\left[[\tilde{a}^{(j_m)} \times a^{(j_m)}]^{(J_1)} \times [a^{(j_p)} \times \tilde{a}^{(j_p)}]^{(x)} \right]^{(J_2)} \times \right. \\ & \left. \times [a^{(j_n)} \times \tilde{a}^{(j_n)}]^{(J_2)} \right]^{(0)} \end{aligned} \quad (15)$$

and

$$\begin{aligned} & \left[\left[[a^{(j_n)} \times \tilde{a}^{(j_m)}]^{(k)} \times [a^{(j_p)} \times \tilde{a}^{(j_p)}]^{(x)} \right]^{(k')} \times \right. \\ & \left. \times [a^{(j_m)} \times \tilde{a}^{(j_n)}]^{(k')} \right]^{(0)} = (-1)^{j_m + j_n + k + x} \sqrt{[k, k']} \times \\ & \times \sum_{J_1, J_2} \sqrt{[J_1, J_2]} \left\{ \begin{matrix} j_m & j_n & k \\ J_1 & J_2 & x \\ j_m & j_n & k' \end{matrix} \right\} \times \left[\left[[\tilde{a}^{(j_m)} \times a^{(j_m)}]^{(J_1)} \times \right. \right. \\ & \left. \left. \times [a^{(j_p)} \times \tilde{a}^{(j_p)}]^{(x)} \right]^{(J_2)} \times [a^{(j_n)} \times \tilde{a}^{(j_n)}]^{(J_2)} \right]^{(0)}. \end{aligned} \quad (16)$$

The program library `librang` [9] available in the GRASP package is sufficient for the calculation of the reduced matrix element of Feynman diagrams A_5 , but the method of the calculation of this type of an operator is not described in the paper [9]. We will now discuss it.

Since we can schematically rewrite the tensorial product as the tensorial product of three operators $A^{(J_1)}(n_m j_m)$, $B^{(x)}(n_p j_p)$ and $C^{(J_2)}(n_n j_n)$ acting on different subshells

$$[A^{(J_1)}(n_m j_m) \times B^{(x)}(n_p j_p)]^{(J_2)} \times C^{(J_2)}(n_n j_n)]^{(0)}, \quad (17)$$

the algebraic expression of the recoupling matrix in this case is given in the paper [11], (Eq. (24) there) and is computed by the subroutine REC3 (Ref. [9], Section 3.2.5). Therefore, the existing capabilities of the library `librang` are fully sufficient for calculating $R(\lambda_i, \lambda_j, \lambda'_i, \lambda'_j, \Lambda^{bra}, \Lambda^{ket}, \Gamma)$.

As far as the submatrix element $T(n_i \lambda_i, n_j \lambda_j, n'_i \lambda'_i, n'_j \lambda'_j, \Lambda^{bra}, \Lambda^{ket}, \Xi, \Gamma)$ is concerned, the situation is different. In this case, the tensorial product can be split into three parts $A^{(J_1)}(n_m j_m)$, $B^{(x)}(n_p j_p)$ and $C^{(J_2)}(n_n j_n)$, where each of these can be expressed as

$$A^{(J_1)}(n_m j_m) = [\tilde{a}^{(j_m)} \times a^{(j_m)}]^{(J_1)} \quad (18)$$

and

$$B^{(k)}(n_j) = C^{(k)}(n_j) = [a^{(j)} \times \tilde{a}^{(j)}]^{(k)}. \quad (19)$$

These parts can be considered separately (because they act on different subshells, and the binding of the ranks of the tensorial structure is already included in the recoupling matrix). Subroutine WJ1 (Ref. [9], Section 3.3.3) finds the matrix element of the operator (17).

The phase factor Δ is zero in this case.

The $\Theta'(n_i \lambda_i, n_j \lambda_j, n'_i \lambda'_i, n'_j \lambda'_j, \Xi)$, which is proportional to the radial part, is found in a regular way as it was found in the papers [1–4].

3.2.2. The exchange part of the fourth type of valence–valence correlations

Now let us discuss the diagram A_6 , with a tensorial structure

$$[[[a_1^{(j_n)} \times \tilde{a}_2^{(j_m)}]^{(k)} \times [a_3^{(j_p)} \times \tilde{a}_4^{(j_n)}]^{(x)}]^{(k')} \times [a_5^{(j_m)} \times \tilde{a}_6^{(j_p)}]^{(k')}]^{(0)}. \quad (20)$$

This tensorial product is not appropriate to calculate the spin-angular part for the same reason as for Eqs. (5) and (13). Therefore, this tensorial product has to be transformed into the following, using the commutation rules of secondary quantization:

$$[[[\tilde{a}_2^{(j_m)} \times a_5^{(j_m)}]^{(J_1)} \times [a_3^{(j_p)} \times \tilde{a}_6^{(j_p)}]^{(y)}]^{(J_2)} \times [a_1^{(j_n)} \times \tilde{a}_4^{(j_n)}]^{(J_2)}]^{(0)}. \quad (21)$$

In this case, the transformation of the tensorial product from Eq. (20) to Eq. (21) results in only one member in Eq. (21), where the transformation matrix of the tensorial structure is shown graphically in Fig. 6. B_4 is proportional to the coefficient $12j$ -symbol [13, 14]. The final expression of this rearrangement of the tensorial structure (20) is the following:

$$\begin{aligned} & \left[[a^{(j_n)} \times \tilde{a}^{(j_m)}]^{(k)} \times [a^{(j_p)} \times \tilde{a}^{(j_n)}]^{(x)} \right]^{(k')} \times \\ & \times [a^{(j_m)} \times \tilde{a}^{(j_p)}]^{(k')} \Big]^{(0)} = \\ & = \sum_{J_1, J_2, y} B_4 \left[[\tilde{a}^{(j_m)} \times a^{(j_m)}]^{(J_1)} \times \right. \\ & \times [a^{(j_p)} \times \tilde{a}^{(j_p)}]^{(y)} \Big]^{(J_2)} \times [a^{(j_n)} \times \tilde{a}^{(j_n)}]^{(J_2)} \Big]^{(0)}. \quad (22) \end{aligned}$$

and

$$\begin{aligned} & \left[[a^{(j_n)} \times \tilde{a}^{(j_m)}]^{(k)} \times [a^{(j_p)} \times \tilde{a}^{(j_p)}]^{(x)} \right]^{(k')} \times \\ & \times [a^{(j_m)} \times \tilde{a}^{(j_n)}]^{(k')} \Big]^{(0)} = (-1)^{j_m + j_p + k' + 1} \sqrt{[k, k', x]} \times \\ & \times \sum_{J_1, J_2, y} (-1)^{J_1 + J_2} \sqrt{[J_1, J_2, y]} \times \\ & \times \left[[\tilde{a}^{(j_m)} \times a^{(j_m)}]^{(J_1)} \times [a^{(j_p)} \times \tilde{a}^{(j_p)}]^{(y)} \right]^{(J_2)} \times \\ & \times [a^{(j_n)} \times \tilde{a}^{(j_n)}]^{(J_2)} \Big]^{(0)} \times \\ & \times \sum_z [z] \begin{Bmatrix} J_1 & j_n & z \\ j_n & y & J_2 \end{Bmatrix} \begin{Bmatrix} y & j_n & z \\ x & j_p & j_p \end{Bmatrix} \begin{Bmatrix} j_p & x & z \\ k & j_m & k' \end{Bmatrix} \begin{Bmatrix} j_m & k & z \\ j_n & J_1 & j_m \end{Bmatrix}. \quad (23) \end{aligned}$$

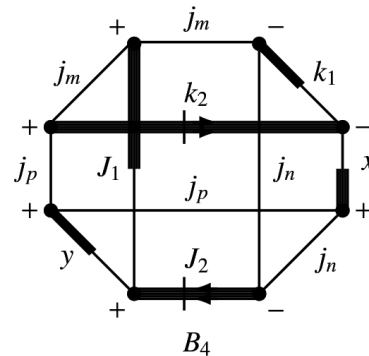


Fig. 6. Diagram showing the recoupling coefficient B_4 of the tensorial product from Eq. (20) to Eq. (21).

The program library `librang` [9] available in the GRASP package is sufficient for the calculation of the reduced matrix element of the Feynman diagram A_6 . The use of the library in this case is exactly the same as the one presented in Subsection 3.2.1, dealt with in the diagram A_5 . In this case, only the multiplier $\Theta'(n_i \lambda_i, n_j \lambda_j, n_i \lambda'_i, n_j \lambda'_j, \Xi)$ differs.

3.2.3. The special cases of fourth type of valence–valence correlations

The way to calculate the reduced matrix elements of Feynman diagrams A_5 and A_6 in the general case is presented in Subsections 3.2.1 and 3.2.2. But it is possible to extract, as it was shown in Subsection 3.1, the individual parts which are more straightforward to calculate, i.e. the coefficient $\Delta \mathcal{E}_0$ (does not depend on the term) and $\Delta \mathcal{F}^k(n, p)$ (regular spin-angular library `librang` can be used). The extraction of these expressions is the same as in the papers [1–4]. Therefore, only the reduced matrix element of part of Feynman diagrams A_5 and A_6 is calculated from the general expressions, where the rank $k > 0$. The part which is calculated from the general expression will be denoted by $\Delta \tilde{\mathcal{R}}^{(k, k', x)}(mnp)$ in the future.

In the next section, we will give the final expressions for these two types of correlations (third and fourth types of valence–valence correlations), as we did in the papers [1–4].

4. Combination of relativistic configuration interaction approximation with the stationary second-order Rayleigh–Schrödinger many-body perturbation theory

Similar to CV, C, CC, and VV correlations [1–4], the admixed configurations from the VV correlations deriving from the three-particle Feynman diagram VV_3 (Eqs. (1) and (4)) can be added to the usual energy $E_0(K)$ of the term χJ of the configuration K and can be expressed as the energy $\Delta \mathcal{E}_0(KJ)$, which does not depend on the term, and the sum of the products of Slater integrals and spin-angular coefficients, describing the interaction within and between the open subshells,

$$E(K \chi J) = E_0(KJ) + \Delta \mathcal{E}_0(KJ) + \sum_{n \ell j} \sum_{k > 0} \tilde{f}_k(\ell j^w, K \chi J) [\mathcal{F}^k(n \ell j, n \ell j) + \Delta \mathcal{F}^k(n \ell j, n \ell j)] +$$

$$+ \sum_{n \ell j} \sum_{n' \ell' j' > n \ell j} \left\{ \sum_{k > 0} \tilde{f}_k(\ell j^w \ell' j'^w, K \chi J) [\mathcal{F}^k(n \ell j, n' \ell' j') + \Delta \mathcal{F}^k(n \ell j, n' \ell' j')] + \right. \\ + \sum_k \tilde{g}_k(\ell j^w \ell' j'^w, K \chi J) \mathcal{G}^k(n \ell j, n' \ell' j') + \\ + \sum_k \tilde{v}_k(\ell j^w \ell' j'^w, \ell j^{w-2} \ell' j'^{w+2}, K \chi J K' \chi' J') \times \\ \left. \times \mathcal{R}^k(n \ell j n \ell j, n' \ell' j' n' \ell' j') \right\} + \\ + \sum_{n \ell j} \sum_{\substack{k > 0 \\ n' \ell' j' \neq n \ell j}} \left\langle \Psi \left\| \left[[\tilde{a}^{(j)} \times a^{(j)}]^{(k)} \times [a^{(j')} \times \tilde{a}^{(j')}]^{(x)} \times \right. \right. \right. \\ \left. \left. \left. \times [a^{(j')} \times \tilde{a}^{(j')}]^{(k')} \right]^{(0)} \right\| \Psi \right\rangle \times \\ \times \Delta \tilde{\mathcal{R}}^{(k, k', x)}(n \ell j n' \ell' j' n' \ell' j') + \\ + \sum_{n \ell j} \sum_{\substack{k > 0 \\ n' \ell' j' \neq n \ell j \\ n'' \ell'' j'' \neq n \ell j}} \left\langle \Psi \left\| \left[[\tilde{a}^{(j)} \times a^{(j)}]^{(k)} \times [a^{(j'')} \times \tilde{a}^{(j'')}]^{(x)} \right]^{(k')} \times \right. \right. \\ \left. \left. \times [a^{(j')} \times \tilde{a}^{(j')}]^{(k')} \right]^{(0)} \right\| \Psi \right\rangle \times \\ \times \Delta \tilde{\mathcal{R}}^{(k, k', x)}(n \ell j n' \ell' j' n'' \ell'' j''), \quad (24)$$

where \tilde{f}_k , \tilde{g}_k and \tilde{v}_k are spin-angular coefficients from which submatrix elements $\langle \ell j \| C^{(k)} \| \ell' j' \rangle$ are extracted. Therefore, the summation over k runs over all possible values instead of the values which satisfy the triangular condition $(\ell \ell' k)$ as it is in the ordinary case. $\mathcal{F}^k(n \ell j, n' \ell' j')$, $\mathcal{G}^k(n \ell j, n' \ell' j')$ and $\mathcal{R}^k(n \ell j n \ell j, n' \ell' j' n' \ell' j')$ are the generalized integrals of the electrostatic interaction between electrons. The definition of $\mathcal{R}^k(n \ell j n \ell j, n' \ell' j' n' \ell' j')$ is the following:

$$\mathcal{R}^k(ij, i'j') = \{ [1 + \delta(i, j)] [1 + \delta(i', j')] \}^{-1/2} R^k(n_i j_i n_j j_j, n_i j_i n_j j_j) \\ \times \langle \ell_i j_i \| C^{(k)} \| \ell_i j_i \rangle \langle \ell_j j_j \| C^{(k)} \| \ell_j j_j \rangle, \quad (25)$$

where $R^k(n_i j_i n_j j_j, n_i j_i n_j j_j)$ is the same radial integral as in Eq. (3). Definitions $\mathcal{F}^k(n \ell j, n' \ell' j')$ and $\mathcal{G}^k(n \ell j, n' \ell' j')$ straightforwardly follow from Eq. (25). Due to the inherent complexity of the three-particle operator, Eq. (24) does not fully distinguish all the members that are independent of the term. Therefore, a very small number of them are retained in the members $\Delta \tilde{\mathcal{R}}^{(k, k', x)}(n \ell j n' \ell' j' n' \ell' j')$ and $\Delta \tilde{\mathcal{R}}^{(k, k', x)}(n \ell j n' \ell' j' n'' \ell'' j'')$.

The contribution deriving from the VV correlations of the configurations K' to $E(K \chi J)$ in

Table 1. Expressions for valence–valence corrections to the energy in Eqs. (24) and (26), independent of the term.

$\Delta\mathcal{E}_0$ corrections
$\overbrace{(n_m \ell_m) j_m^{w_m} (n_n \ell_n) j_n^{w_n}}^{\text{valence subshells}} \rightarrow \overbrace{(n_m \ell_m) j_m^{w_m+1} (n_n \ell_n) j_n^{w_n-2}}^{\text{valence subshells}} \overbrace{(n_r \ell_r) j_r}^{\text{virtual subshell}}$ $-\frac{2([j_m]-w_m)w_n(w_n-1)}{[j_m, j_n]} \mathcal{A}'(0, nn, mr)$ <p style="text-align: center;">from VV_3 Feynman diagram</p>
$\overbrace{(n_m \ell_m) j_m^{w_m} (n_n \ell_n) j_n^{w_n} (n_p \ell_p) j_p^{w_p}}^{\text{valence subshells}} \rightarrow \overbrace{(n_m \ell_m) j_m^{w_m+1} (n_n \ell_n) j_n^{w_n-1} (n_p \ell_p) j_p^{w_p-1}}^{\text{valence subshells}} \overbrace{(n_r \ell_r) j_r}^{\text{virtual subshell}}$ $-(-1)^{j_m+j_n+j_p+j_r} \frac{([j_m]-w_m)w_n w_p}{[j_m, j_n, j_p]} \sum_k \left\{ \frac{\mathcal{P}(kk, np, mr)}{[k]} + \mathcal{C}(k, np, mr) \right\} (1 + P(n \rightleftharpoons p))$ <p style="text-align: center;">from VV_3 Feynman diagram</p>

the second order of perturbation theory can be extracted from Eq. (24) as

$$\begin{aligned} \Delta E_{PT(VVT)} &= \Delta \mathcal{E}_0(KJ) + \\ &+ \sum_{n\ell j} \sum_{k>0} \tilde{f}_k(\ell j^w, K\chi J) \Delta \mathcal{F}^k(n\ell j, n\ell j) + \\ &+ \sum_{n\ell j} \sum_{n'\ell'j'>n\ell j} \sum_{k>0} \tilde{f}_k(\ell j^w \ell' j'^{w'}, K\chi J) \Delta \mathcal{F}^k(n\ell j, n'\ell'j') + \\ &+ \sum_{n\ell j} \sum_{n'\ell'j' \neq n\ell j} \sum_{k>0} \left\langle \Psi \left\| \left[\tilde{a}^{(j)} \times a^{(j)} \right]^{(k)} \times \right. \right. \\ &\quad \times \left. \left[a^{(j')} \times \tilde{a}^{(j')} \right]^{(x)} \times \left[a^{(j')} \times \tilde{a}^{(j')} \right]^{(k')} \right]^{(k)} \right\rangle^{(0)} \left\| \Psi \right\rangle \\ &\quad \times \Delta \tilde{\mathcal{R}}^{(k,k',x)}(n\ell j, n'\ell'j', n'\ell'j') \\ &\quad + \sum_{n\ell j} \sum_{n'\ell'j' \neq n\ell j} \sum_{k>0} \left\langle \Psi \left\| \left[\left[\tilde{a}^{(j)} \times a^{(j)} \right]^{(k)} \times \left[a^{(j')} \times \tilde{a}^{(j')} \right]^{(x)} \right]^{(k')} \times \right. \right. \\ &\quad \times \left. \left[a^{(j')} \times \tilde{a}^{(j')} \right]^{(k')} \right]^{(0)} \right\| \Psi \rangle \times \\ &\quad \times \Delta \tilde{\mathcal{R}}^{(k,k',x)}(n\ell j, n'\ell'j', n''\ell''j''). \end{aligned} \quad (26)$$

Table 2. Expressions for Slater integrals $\Delta \mathcal{F}^k(n, n)$, $\Delta \mathcal{F}^k(m, n)$ and $\Delta \tilde{\mathcal{R}}^{(k,k',x)}(mnn)$ (see Eqs. (24) and (26)) corrections corresponding to the third type of valence–valence correlations.

Corrections	Slater integral	k values
$\overbrace{-4[k] \frac{([j_m]-w_m)}{[j_m]} \mathcal{A}'(k, nn, mr)}^{\text{from } VV_3 \text{ Feynman diagram}}$	$\Delta \mathcal{F}^k(n, n)$	$k > 0$
$\overbrace{2[k] \sum_{k'} (-1)^{j_n+j_r+k'} \left\{ \begin{matrix} j_m & j_m & k \\ j_n & j_n & k' \end{matrix} \right\} \mathcal{C}(k', rm, nn)}^{\text{from } VV_3 \text{ Feynman diagram}}$	$\Delta \mathcal{F}^k(m, n)$	$k > 0$
$\overbrace{2(-1)^{-j_m+j_n+x} \sqrt{[k, k', x]} \mathcal{G}(k, k', x, nn, mr)}^{\text{from } VV_3 \text{ Feynman diagram}}$	$\Delta \tilde{\mathcal{R}}^{(k,k',x)}(mnn)$	$k > 0$

The contribution of the third and fourth type of the VV correlations in the second order of perturbation theory is expressed over $\Delta\mathcal{E}_0(KJ)$, $\Delta\mathcal{F}^k(nlj, nlj)$, $\Delta\mathcal{F}^k(nlj, n'l'j')$, $\Delta\tilde{\mathcal{R}}^{(k, k', x)}(nlj, n'l'j', n'l'j')$ and $\Delta\tilde{\mathcal{R}}^{(k, k', x)}(nlj, n'l'j', n''l''j'')$ (see Tables 1, 2 and 3). These formulae are additionally expressed via the quantities

$$\mathcal{A}(x, ij, i'j') = \sum_{k, k'} \left\{ \begin{matrix} k & k' & x \\ j_i & j_i & j_{i'} \end{matrix} \right\} \left\{ \begin{matrix} k & k' & x \\ j_j & j_j & j_{j'} \end{matrix} \right\} \mathcal{P}(kk', ij, i'j'), \quad (27)$$

$$\mathcal{C}(k, ij, i'j') = \sum_{k'} \left\{ \begin{matrix} k & j_i & j_{i'} \\ k' & j_j & j_{j'} \end{matrix} \right\} Q(kk', ij, i'j'), \quad (28)$$

and

$$\mathcal{G}(x_1 x_2 x, ij, i'j') = \sum_{k, k'} (-1)^{k'} \left\{ \begin{matrix} j_j & j_j & x \\ k & k' & j_{j'} \end{matrix} \right\} \left\{ \begin{matrix} j_{i'} & j_i & k \\ x_1 & x_2 & x \\ j_{i'} & j_i & k' \end{matrix} \right\} \mathcal{P}(kk', ij, i'j'), \quad (29)$$

where

$$\mathcal{P}(kk', ij, i'j') = \mathcal{R}^k(ij, i'j') \mathcal{R}^{k'}(i'j', ij) \mathcal{O}(K', K), \quad (30)$$

$$Q(kk', ij, i'j') = \mathcal{R}^k(ij, i'j') \mathcal{R}^{k'}(i'j', ji) \mathcal{O}(K', K), \quad (31)$$

$$\mathcal{O}(K', K) = \frac{1}{\bar{E}(K') - \bar{E}(K)}, \quad (32)$$

where $\bar{E}(K)$ is the averaged energy of the state for which calculations are performed. $\bar{E}(K')$ is the

Table 3. Expressions for Slater integrals $\Delta\mathcal{F}^k(n, p)$ and $\Delta\tilde{\mathcal{R}}^{(k, k', x)}(mnp)$ (see Eqs. (24) and (26)) corrections corresponding to the fourth type of valence–valence correlations.

Corrections	Slater integral	k values
$\underbrace{\overbrace{(n_m \ell_m) j_m^{w_m} (n_n \ell_n) j_n^{w_n} (n_p \ell_p) j_p^{w_p}}^{\text{valence subshells}} \rightarrow \overbrace{(n_m \ell_m) j_m^{w_m+1} (n_n \ell_n) j_n^{w_n-1} (n_p \ell_p) j_p^{w_p-1}}^{\text{valence subshells}} \overbrace{(n_r \ell_r) j_r}^{\text{virtual subshell}}}_{\text{from VV}_3 \text{ Feynman diagram}} \underbrace{(-1)^{j_m+j_n} [k] \sqrt{[k]} \frac{([j_m] - w_m)}{\sqrt{[j_m]}} \{(-1)^{k+1} \mathcal{G}(0 k k, np, mr)\}}_{\Delta\mathcal{F}^k(n, p)} \quad k > 0$ $+ \underbrace{\sum_{k_1, k_2, k_3} (-1)^{k_1+k} [k_3] \left\{ \begin{matrix} j_n & j_p & k_3 \\ k_1 & k_2 & j_r \end{matrix} \right\} Q(k_1 k_2, np, mr)}_{\text{from VV}_3 \text{ Feynman diagram}}$ $\times \underbrace{\mathcal{C}_{12j}(j_m j_n j_p, k_1 k_2 k_3, 0 k k) \left\{ 1 + \text{P} \left(\begin{matrix} n \rightleftharpoons p \\ k_1 \rightleftharpoons k_2 \end{matrix} \right) \right\}}_{\text{from VV}_3 \text{ Feynman diagram}}$		
$\underbrace{(-1)^{j_m+j_n} \sqrt{[k, k', x]} \{(-1)^{x+1} \mathcal{G}(kk' x, np, mr)\}}_{\text{from VV}_3 \text{ Feynman diagram}} \quad \Delta\tilde{\mathcal{R}}^{(k, k', x)}(mnp) \quad k > 0$ $+ \underbrace{\sum_{k_1, k_2, k_3} (-1)^{k+k'+k_1} [k_3] \left\{ \begin{matrix} j_n & j_p & k_3 \\ k_1 & k_2 & j_r \end{matrix} \right\} Q(k_1 k_2, np, mr)}_{\text{from VV}_3 \text{ Feynman diagram}}$ $\times \underbrace{\mathcal{C}_{12j}(j_m j_n j_p, k_1 k_2 k_3, k k' x) \left\{ 1 + \text{P} \left(\begin{matrix} n \rightleftharpoons p \\ k_1 \rightleftharpoons k_2 \\ k' \rightleftharpoons x \end{matrix} \right) \right\}}_{\text{from VV}_3 \text{ Feynman diagram}}$		

averaged energy for the admixed configuration K' . For details on how to find $\bar{E}(K)$ and $\bar{E}(K')$, see Ref. [1], Section 3. We would like to emphasize that the energy denominator (32) is defined differently/opposite to the expressions of Feynman diagrams (see Fig. 1, Eqs. (30, 31)):

$$\begin{aligned} \mathcal{C}_{12j}(iji', k_1 k_2 k_3, J_1 J_2 J) = \\ = \sum_x [x] \begin{Bmatrix} J_1 & j_j & x \\ j_j & J & J_2 \end{Bmatrix} \begin{Bmatrix} J & j_j & x \\ k_3 & j_{i'} & j_{i'} \end{Bmatrix} \times \\ \times \begin{Bmatrix} j_{i'} & k_3 & x \\ k_1 & j_i & k_2 \end{Bmatrix} \begin{Bmatrix} j_i & k_1 & x \\ j_j & J_1 & j_i \end{Bmatrix}. \end{aligned} \quad (33)$$

We would also like to point out that the notation of ranks such as J, J_2, y in the multipliers of this section under $\Delta\tilde{\mathcal{R}}^{(k, k', x)}(mnn)$ and $\Delta\tilde{\mathcal{R}}^{(k, k', x)}(mnp)$ have been renamed for convenience to make the expressions in Tables 2 and 3 more straightforward and more understandable.

This theory in an irreducible tensorial form, as in the papers [1–4], is more suitable to be included in such a version of the GRASP which is based on configuration state function generators [19, 20]. This is related to the fact that this version of the software package allows us to easily distinguish the F, F' and G sets of orbitals in the process of computing atomic data. In the following section, we will present a test case of this implementation.

5. Calculation of core–valence, core and valence–valence (including these which are described by the three-particle Feynman diagram) correlations with a new approach

The computations in the present work were performed in the regular way and using the method based on the Rayleigh–Schrödinger perturbation theory in an irreducible tensorial form [1–4], which was extended to include VV correlations described by the three-particle Feynman diagram (VVT). The developed RSMBPT method was applied to select the most significant configuration state functions. For the first time in this work, the configuration state function (CSF) bases constructed using the RSMBPT method were used to solve the self-consistent field equations. It should be mentioned that in the previous studies [1–4, 22], the RSMBPT method was only applied with

relativistic configuration interaction (RCI). In the case of the regular calculations, to include different types of correlations in the multiconfiguration Dirac–Hartree–Fock (MCDHF) calculations often is a complex task, or even impossible, due to time and computer resource limitations, especially for complex systems. Basically, only VV correlations and additionally some limited correlations from the core (if the CSF bases are not too large) are included in these calculations. The application of the RSMBPT method for solving self-consistent field equations allows one to include the most important correlations of various types.

For such investigations, the energy structure calculations were performed for the 105 lowest energy levels of the $4s^2 4p^2, 4p^4, 4s^2 4p\{4d, 4f, 5s, 5p, 5d, 6s, 6p\}, 4s4p^3$ and $4s4p^2\{4d, 5s\}$ configurations of the Se III using the regular way and the RSMBPT method when CV, C, VV and VVT correlations were included. In further description, the VV correlations investigated in Ref. [4] and the VV correlations described by the three-particle Feynman diagram (VVT) investigated in this work will be marked as VV. The multireference (MR) set in the present calculations consists of the $4s^2 4p^2, 4p^4, 4s^2 4p\{4f, 5p, 6p\}, 4s4p^2\{4d, 5s\}$ even and $4s^2 4p\{4d, 5s, 5d, 6s\}, 4s4p^3$ odd configurations. Firstly, the MCDHF calculation for the even and odd states of the configurations belonging to the MR set was done in the extended optimal level (EOL) scheme [21]. These radial wavefunctions were used for further investigations. The initial calculation was followed by separate calculations in the EOL scheme for the even and odd parity states using the regular way and the RSMBPT method. These calculations are described in the subsections below, and the results are presented in Section 5.2. The calculations using both methods were performed including only CSFs that have non-zero matrix elements in the sets of spin-angular integration with the CSFs belonging to the configurations in the MR set. At the RCI calculations step, the Breit interactions and leading quantum electrodynamic effects – the vacuum polarization and self-energy corrections – were included.

5.1. Computational schemes

5.1.1. Regular GRASP2018 calculations

Regular MCDHF computations including the CV, C and VV correlations are marked as **CV+C+VV**

MCDHF. In this computational scheme, single-double (SD) substitutions are allowed from the 4s, 4p₊, 4p₋, 4d₊, 4d₋, 4f₊, 4f₋, 5s, 5p₊, 5p₋, 5d₊, 5d₋, 6s, 6p₊, 6p₋ valence orbitals of the MR set and the S substitutions from the 3s, 3p₊, 3p₋, 3d₊ and 3d₋ core orbitals to the orbital set (OS) $OS_1 = \{7s, 7p_+, 7p_-, 6d_+, 6d_-, 5f_+, 5f_-, 5g_+, 5g_-\}$, $OS_2 = \{8s, 8p_+, 8p_-, 7d_+, 7d_-, 6f_+, 6f_-, 6g_+, 6g_-\}$. The 1s, 2s, 2p₊ and 2p₋ subshells are defined as inactive core subshells. The radial wavefunctions of the new OS are estimated using the Thomas–Fermi potential and further self-consistent field equations are solved. When a new OS is computed, the previous orbitals are frozen. Based on the orbitals from the MCDHF calculations, further RCI calculations are performed. Regular RCI calculations are marked as **CV+C+VV RCI**.

5.1.2. Calculations using the RSBMBPT method

The CSF space in the computations using the RSBMBPT method is divided into three sets: F , F' and G (see Ref. [1] for details). The 1s, 2s, 2p₊ and 2p₋ subshells are defined as inactive core subshells in the calculations, the same as it is done in the regular GRASP2018 calculations. The 3s, 3p₊, 3p₋, 3d₊ and 3d₋ subshells are defined as core subshells (that correspond to F set), 4s, 4p₊, 4p₋, 4d₊, 4d₋, 4f₊, 4f₋, 5s, 5p₊, 5p₋, 5d₊, 5d₋, 6s, 6p₊, 6p₋ as valence subshells (that correspond to F' set) and subshells belonging to OS_1 and OS_2 as virtual ones (that correspond to G set). Such space distribution is consistent with the regular GRASP2018 calculations described above.

The RSBMBPT calculation procedure is analogous to that used in the previous research [1–4]. The contribution of each K' configuration for CSF for which energy needs to be calculated according to Rayleigh–Schrödinger perturbation theory in an irreducible tensorial form is computed according to Eq. (22) of Ref. [1] (for CV correlations), Eq. (6) of Ref. [2] (for C correlations), Eq. (19) of Ref. [4] (for VV correlations) and Eq. (26) (for VVT correlations). K' configurations are sorted in a descending order according to the impact of the correlations for each level. Further, K' configurations are selected by CV, C and VV correlations impact with the specified fraction (expressed in the percentage: 95, 99, 99.5, 99.95 and 100%) of the total correlations contribution. It should be noted that the program gives the contribution of the correlations of K' configuration with a value greater than

1.0E-11. Contributions of smaller magnitudes are neglected. The estimation of the correlations using the stationary second-order Rayleigh–Schrödinger many-body perturbation theory in an irreducible tensorial form is done for the Coulomb interaction. The C correlations (Eq. (3) of Ref. [2]) and CV correlations (Eq. (4) of Ref. [2]), which are not included with the RSBMBPT method, were added to the calculations in a regular way.

Firstly, the radial wavefunctions of OS_1 are estimated using the Thomas–Fermi potential. Then using the RSBMBPT method, the CSF basis is constructed by selecting the most important CV, C and VV correlations with the specified fraction (95, 99, 99.5, 99.95 and 100%) for the even and odd parities. The self-consistent field equations are solved with the CSF basis for the specified fraction. The computed radial wavefunctions are taken as initial and the selection procedure of the most significant CV, C and VV correlations using the RSBMBPT method is performed for the construction of CSF basis. The variation and selection of CSFs is repeated a few times to reach the convergence. The results of these investigations will be presented in the next section. Further the radial wavefunctions of OS_2 are computed. In this step, firstly the radial wavefunctions of OS_1 and OS_2 are estimated using the Thomas–Fermi potential and the selection procedure of the most important correlations from OS_1 and OS_2 is performed. This is done so that the contribution of CSFs from both (OS_1 and OS_2) sets would be estimated with similar accuracy radial wavefunctions. The constructed CSF basis is used to solve self-consistent field equations for OS_2 , in which the radial wavefunctions of OS_1 are taken from the final OS_1 calculations and are frozen. The computed radial wavefunctions are taken as initial and the selection procedure of CSFs followed by a solution of the self-consistent field equations is repeated a few times to achieve the convergence, as it was done for OS_1 . The results from MCDHF computations including CV, C and VV correlations according to the RSBMBPT method are marked as **CV+C+VV MCDHF (RSMBPT)**.

RCI computations are performed for the OS_1 and OS_2 taking the radial wavefunctions from the specified fraction (95, 99, 99.5, 99.95 and 100%) MCDHF calculations and the CSF basis from the regular GRASP2018 calculations. Additionally, for the OS_2 RCI calculations are performed taking the radial

wavefunctions from the specified fraction (95, 99, 99.5 and 99.95%) MCDHF calculations and the CSF basis constructed using the RSMBPT method with the same specified fraction (95, 99, 99.5 and 99.95%) as in MCDHF. The results including CV, C and VV correlations according to the RSMBPT method are marked as **CV+C+VV RCI (RSMBPT)**.

5.2. Results

5.2.1. Results from MCDHF calculations

This section presents the results of the investigation of the RSMBPT method for solving self-consistent field equations. These results are also compared with the regular GRASP2018 calculations. In Table 4, the SELF-CONSISTENCY and NORM-1 parameters [23] from the MCDHF equations solutions for the OS_1 of the even parity states in 95, 99, 99.5,

99.95, 100% and regular cases are presented. For each step of variation, the initial and final results of these parameters are given. As seen from Table 4, these parameters converge with each variation step, and after a few variations, the initial and final results almost do not change in the case of 100%. In other cases of 95, 99, 99.5 and 99.95%, the convergence is slower, so more variation steps are needed. The final SELF-CONSISTENCY and NORM-1 parameters are also very good when the most important CV+C+VV correlations with the specified fraction (95, 99, 99.5 and 99.95%) are included in the computations. In these cases, the CSF basis decreases by up to several times compared to the regular calculations. Similar trends are observed for the OS_1 of odd parity, also for the OS_2 of both even and odd parity, therefore only the results for the boundary computed cases are presented in Tables 5–7.

Table 4. SELF-CONSISTENCY and NORM-1 parameters solving the MCDHF equations of the OS_1 for even parity states in 95, 99, 99.5, 99.95, 100% and regular cases. Columns with ‘x’ var. mean the number of variations with the constructed CSF basis. In. and Fin. mean the initial and final results of these parameters solving the MCDHF equations.

Subshell	1 var.		2 var.		3 var.		4 var.	
	In.	Fin.	In.	Fin.	In.	Fin.	In.	Fin.
SELF-CONSISTENCY in case 95%								
7s	1.81E-02	2.64E-06	2.28E-04	4.33E-07	5.38E-06	3.79E-07	1.67E-06	8.78E-08
7p ₋	1.15E-02	3.14E-06	1.27E-03	3.15E-07	4.69E-05	3.75E-07	6.12E-06	1.63E-07
7p ₊	1.90E-02	3.92E-06	1.00E-03	4.43E-07	6.31E-05	5.47E-07	4.24E-06	1.70E-07
6d ₋	3.98E-02	3.11E-06	8.25E-04	3.94E-07	3.24E-05	3.95E-07	1.54E-06	1.31E-07
6d ₊	5.43E-02	3.86E-06	7.64E-04	4.15E-07	5.49E-05	4.54E-07	5.82E-06	1.40E-07
5f ₋	2.10E-02	1.02E-06	1.14E-03	9.71E-08	5.72E-05	1.34E-07	1.26E-05	1.02E-07
5f ₊	2.66E-02	1.33E-06	1.03E-03	1.10E-07	8.63E-05	1.95E-07	1.26E-05	9.47E-08
5g ₋	8.45E-03	1.15E-07	4.24E-04	1.90E-08	5.72E-05	1.45E-07	7.87E-07	8.94E-09
5g ₊	9.43E-03	1.24E-07	4.46E-04	1.33E-08	3.22E-05	4.11E-08	3.22E-08	1.28E-08
NORM-1 in case 95%								
7s	3.78E-01	-3.58E-05	-2.72E-03	-5.36E-06	6.35E-05	-4.69E-06	1.76E-05	-1.12E-06
7p ₋	1.44E-01	-2.25E-05	-9.27E-03	-3.82E-06	-4.61E-04	-4.38E-06	-6.77E-05	-1.81E-06
7p ₊	1.57E-01	-2.86E-05	-6.43E-03	-3.47E-06	-4.94E-04	-4.58E-06	-3.22E-05	-1.41E-06
6d ₋	1.35E-01	-1.60E-05	-4.55E-03	-2.47E-06	-7.01E-06	-2.25E-06	4.48E-06	-7.90E-07
6d ₊	1.67E-01	-1.70E-05	-2.03E-03	-1.99E-06	-1.25E-05	-2.05E-06	3.47E-06	-6.43E-07
5f ₋	8.54E-02	-8.77E-06	-7.73E-03	-8.07E-07	-5.17E-04	-1.10E-06	-9.83E-05	-8.04E-07
5f ₊	1.03E-01	-9.51E-06	-5.84E-03	-7.81E-07	-6.61E-04	-1.37E-06	-8.08E-05	-6.57E-07
5g ₋	4.80E-01	3.68E-06	-1.28E-02	6.16E-07	-2.00E-03	-5.38E-06	-2.47E-05	2.81E-07
5g ₊	4.81E-01	3.45E-06	-1.20E-02	3.69E-07	-8.74E-04	-1.38E-06	-7.48E-07	3.76E-07
SELF-CONSISTENCY in case 99%								
7s	1.92E-02	7.24E-07	1.64E-04	9.53E-07	9.41E-06	1.35E-07	7.47E-07	4.56E-08
7p ₋	1.24E-02	6.64E-07	2.68E-04	5.96E-07	5.82E-05	7.63E-08	2.82E-06	1.17E-08
7p ₊	2.11E-02	8.21E-07	3.03E-04	8.41E-07	9.31E-05	1.05E-07	9.87E-07	2.15E-08
6d ₋	2.56E-02	6.85E-07	2.47E-04	3.81E-06	2.96E-04	1.66E-07	1.86E-06	9.85E-08
6d ₊	4.41E-02	8.19E-07	2.41E-04	1.33E-06	2.06E-04	1.70E-07	1.53E-06	9.87E-08
5f ₋	2.24E-02	2.02E-07	3.59E-04	1.62E-06	4.90E-04	5.25E-08	7.38E-06	2.95E-08
5f ₊	2.78E-02	2.48E-07	1.45E-04	9.31E-07	3.17E-04	4.95E-08	3.34E-06	3.02E-08
5g ₋	8.80E-03	4.91E-08	2.15E-03	1.20E-05	1.97E-03	5.89E-08	3.80E-05	8.28E-08
5g ₊	9.88E-03	1.37E-07	3.60E-03	1.22E-06	1.49E-03	4.08E-08	2.87E-05	6.17E-08

Table 4. (Continued)

Subshell	1 var.		2 var.		3 var.		4 var.	
	In.	Fin.	In.	Fin.	In.	Fin.	In.	Fin.
NORM-1 in case 99%								
7s	3.91E-01	-8.96E-06	-2.02E-03	-1.13E-05	7.13E-05	-1.64E-06	-7.87E-06	-5.79E-07
7p	1.59E-01	-7.29E-06	-2.77E-03	-7.13E-06	4.68E-04	-9.49E-07	2.29E-05	-1.87E-07
7p _̄	1.74E-01	-6.59E-06	-2.33E-03	-6.80E-06	6.17E-04	-8.16E-07	5.24E-06	-1.92E-07
6d	6.12E-02	-3.77E-06	-3.08E-04	-2.20E-05	-1.41E-03	-1.00E-06	-9.33E-06	-5.80E-07
6d _̄	1.08E-01	-3.71E-06	-4.03E-04	-6.41E-06	-8.06E-04	-8.36E-07	5.40E-07	-4.62E-07
5f	9.73E-02	-1.65E-06	-2.31E-03	-9.94E-06	4.06E-03	-3.88E-07	4.95E-05	-1.93E-07
5f _̄	1.13E-01	-1.73E-06	-7.25E-04	-5.95E-06	2.23E-03	-3.21E-07	1.99E-05	-1.76E-07
5g	5.00E-01	1.66E-06	-3.60E-02	-4.65E-04	-3.18E-02	-1.38E-06	-8.93E-04	-1.88E-06
5g _̄	5.06E-01	4.27E-06	-4.14E-02	-3.23E-05	-2.05E-02	-8.61E-07	-5.73E-04	-1.25E-06
SELF-CONSISTENCY in case 99.5%								
7s	1.93E-02	6.49E-06	1.15E-04	2.95E-07	5.46E-06	5.36E-07	1.50E-07	1.67E-08
7p	1.26E-02	6.41E-06	1.30E-04	1.92E-07	8.84E-05	9.95E-07	1.45E-06	8.38E-08
7p _̄	2.13E-02	8.14E-06	8.27E-05	2.71E-07	1.09E-04	1.34E-06	6.88E-07	5.94E-08
6d	3.16E-02	6.06E-06	6.97E-05	3.20E-07	5.33E-05	3.97E-07	1.13E-06	2.56E-08
6d _̄	4.21E-02	7.14E-06	6.84E-05	3.70E-07	6.56E-05	4.99E-07	4.49E-07	8.16E-08
5f	2.26E-02	2.02E-06	1.08E-04	1.12E-07	2.66E-04	2.33E-07	1.31E-05	1.21E-07
5f _̄	2.79E-02	2.46E-06	2.86E-05	1.20E-07	2.97E-04	4.18E-07	1.96E-06	2.39E-08
5g	8.96E-03	1.20E-06	3.90E-03	1.45E-07	7.09E-04	1.16E-06	1.02E-05	7.05E-08
5g _̄	1.00E-02	1.55E-06	4.84E-03	1.13E-07	7.95E-04	1.14E-06	2.10E-05	2.03E-07
NORM-1 in case 99.5%								
7s	3.92E-01	-7.81E-05	-1.28E-03	-3.54E-06	-5.68E-05	6.43E-06	1.67E-06	8.67E-08
7p	1.61E-01	-7.22E-05	-1.43E-03	-2.33E-06	6.94E-04	1.03E-05	1.50E-05	8.08E-07
7p _̄	1.76E-01	-6.60E-05	-6.09E-04	-2.17E-06	7.30E-04	1.09E-05	5.30E-06	4.38E-07
6d	8.43E-02	-3.20E-05	-2.60E-04	-1.95E-06	-1.71E-04	-2.88E-07	3.55E-06	-5.37E-08
6d _̄	9.89E-02	-3.10E-05	-1.17E-04	-1.83E-06	-1.76E-04	-5.19E-07	1.40E-06	-2.68E-07
5f	9.88E-02	-1.63E-05	-7.45E-04	-8.47E-07	2.16E-03	1.95E-06	9.44E-05	9.55E-07
5f _̄	1.14E-01	-1.71E-05	-9.50E-05	-7.93E-07	2.06E-03	3.05E-06	1.15E-05	-5.87E-08
5g	5.07E-01	4.29E-05	-4.09E-02	-4.16E-06	-7.40E-03	-2.52E-05	-2.05E-04	-1.42E-06
5g _̄	5.08E-01	4.94E-05	-4.02E-02	-2.81E-06	-8.22E-03	-2.23E-05	-4.16E-04	-4.00E-06
SELF-CONSISTENCY in case 99.95%								
7s	1.94E-02	1.75E-06	2.75E-05	1.79E-07	1.35E-06	4.58E-08	4.49E-08	1.01E-08
7p	1.28E-02	1.37E-06	2.53E-05	1.27E-07	1.97E-05	2.34E-08	2.43E-07	7.49E-09
7p _̄	2.13E-02	1.76E-06	6.87E-05	1.53E-07	1.38E-05	1.78E-08	6.42E-08	3.92E-09
6d	3.38E-02	1.23E-06	1.79E-04	2.51E-07	8.53E-06	1.79E-07	4.04E-08	1.48E-09
6d _̄	4.15E-02	3.24E-06	2.51E-04	1.85E-07	1.17E-05	1.00E-07	1.31E-07	1.60E-09
5f	2.27E-02	7.84E-07	2.80E-04	8.41E-08	5.83E-06	1.10E-07	8.15E-08	3.00E-09
5f _̄	2.80E-02	1.16E-06	3.26E-04	5.49E-08	2.16E-05	5.17E-09	7.15E-07	4.76E-09
5g	9.15E-03	1.73E-06	5.88E-03	1.06E-07	3.92E-04	2.19E-07	7.32E-07	6.65E-09
5g _̄	1.03E-02	2.95E-06	1.56E-03	2.89E-08	4.87E-05	7.88E-09	6.51E-08	1.33E-09
NORM-1 in case 99.95%								
7s	3.93E-01	-2.07E-05	-2.80E-04	-2.16E-06	-1.58E-05	-5.74E-07	-5.60E-07	-7.78E-08
7p	1.61E-01	-1.55E-05	-2.35E-04	-1.47E-06	1.53E-04	-3.07E-07	2.19E-06	-1.29E-08
7p _̄	1.75E-01	-1.41E-05	2.65E-04	-1.16E-06	1.06E-04	-8.40E-09	3.84E-08	2.13E-09
6d	9.46E-02	-6.52E-06	-7.54E-04	-1.51E-06	-5.04E-06	-9.93E-07	-1.77E-07	-2.39E-08
6d _̄	9.57E-02	-1.62E-05	-1.08E-03	-9.25E-07	1.19E-05	-4.52E-07	-3.58E-07	5.35E-10
5f	9.95E-02	-6.06E-06	2.25E-03	-6.12E-07	3.98E-05	-7.68E-07	-4.43E-07	-2.38E-08
5f _̄	1.14E-01	-7.27E-06	2.26E-03	-3.64E-07	1.38E-04	2.05E-08	4.57E-06	3.06E-08
5g	5.13E-01	7.14E-05	-4.42E-02	-2.58E-06	-6.85E-03	-4.94E-06	-1.51E-05	-1.59E-07
5g _̄	5.19E-01	-1.01E-04	-1.92E-02	-6.30E-07	9.48E-04	1.40E-07	8.64E-07	2.64E-08
SELF-CONSISTENCY in case 100%								
7s	1.94E-02	4.89E-07	1.88E-07	2.35E-08	1.36E-08	8.83E-09	9.51E-09	9.53E-09
7p	1.28E-02	4.18E-07	1.35E-07	1.69E-08	1.03E-08	6.14E-09	6.13E-09	6.09E-09
7p _̄	2.13E-02	5.04E-07	3.60E-07	1.30E-08	7.12E-09	1.75E-09	1.11E-09	9.85E-10
6d	3.24E-02	4.18E-07	4.74E-07	5.52E-08	2.02E-08	3.56E-09	1.70E-09	9.10E-10
6d _̄	4.15E-02	5.01E-07	6.14E-07	4.81E-08	1.83E-08	2.93E-09	1.53E-09	4.09E-10
5f	2.28E-02	1.29E-07	1.33E-06	3.12E-08	1.01E-08	1.70E-09	7.70E-10	1.74E-10
5f _̄	2.80E-02	1.48E-07	1.66E-06	1.33E-08	5.49E-09	1.00E-09	7.17E-10	1.62E-10
5g	9.34E-03	7.80E-08	1.26E-04	6.54E-08	2.30E-08	2.62E-09	8.96E-10	2.35E-10
5g _̄	1.04E-02	7.64E-08	8.66E-05	2.27E-08	8.22E-09	9.91E-10	6.20E-10	1.70E-10
NORM-1 in case 100%								
7s	3.93E-01	-5.84E-06	9.35E-07	-3.17E-07	-1.98E-07	-1.08E-07	-9.15E-08	-9.11E-08
7p	1.61E-01	-4.62E-06	-9.80E-07	-2.15E-07	-1.32E-07	-6.79E-08	-5.58E-08	-5.52E-08
7p _̄	1.75E-01	-3.91E-06	-1.72E-06	-1.20E-07	-7.58E-08	-3.25E-08	-2.36E-08	-2.34E-08
6d	8.79E-02	-2.45E-06	-1.03E-06	-3.35E-07	-1.36E-07	-3.99E-08	-2.84E-08	-2.30E-08
6d _̄	9.59E-02	-2.44E-06	-1.77E-06	-2.27E-07	-8.93E-08	-1.66E-08	-9.43E-09	-3.20E-09
5f	9.98E-02	-9.94E-07	-2.54E-06	-2.18E-07	-7.45E-08	-1.60E-08	-8.72E-09	-3.90E-09
5f _̄	1.14E-01	-9.86E-07	-7.48E-06	-7.72E-08	-3.42E-08	-6.92E-09	-4.82E-09	5.80E-10

Table 4. (Continued)

Subshell	1 var.		2 var.		3 var.		4 var.	
	In.	Fin.	In.	Fin.	In.	Fin.	In.	Fin.
5g	5.26E-01	-1.88E-06	-1.58E-03	-1.47E-06	-5.10E-07	-7.15E-08	-3.15E-08	-1.50E-08
5g	5.28E-01	-1.66E-06	-1.90E-04	-4.56E-07	-1.64E-07	-2.25E-08	-1.47E-08	1.37E-09
SELF-CONSISTENCY in case regular								
7s	1.94E-02	4.89E-07						
7p	1.28E-02	4.18E-07						
7p	2.13E-02	5.04E-07						
6d	3.24E-02	4.16E-07						
6d	4.15E-02	5.00E-07						
5f	2.28E-02	1.29E-07						
5f	2.80E-02	1.47E-07						
5g	9.34E-03	7.36E-08						
5g	1.04E-02	7.39E-08						
NORM-1 in case regular								
7s	3.93E-01	-5.83E-06						
7p	1.61E-01	-4.62E-06						
7p	1.75E-01	-3.90E-06						
6d	8.79E-02	-2.44E-06						
6d	9.59E-02	-2.43E-06						
5f	9.97E-02	-9.92E-07						
5f	1.14E-01	-9.83E-07						
5g	5.26E-01	-1.73E-06						
5g	5.28E-01	-1.57E-06						

Table 5. SELF-CONSISTENCY and NORM-1 parameters solving the MCDHF equations of the OS_1 for odd parity states in 95, 100% and regular cases. Columns marked as in Table 4.

Subshell	1 var.		2 var.		3 var.		4 var.	
	In.	Fin.	In.	Fin.	In.	Fin.	In.	Fin.
SELF-CONSISTENCY in case 95%								
7s	1.92E-02	1.08E-07	4.18E-04	4.77E-07	8.10E-06	1.39E-06	8.11E-07	5.80E-08
7p	1.16E-02	8.61E-07	1.26E-03	2.79E-07	9.60E-05	7.68E-07	1.23E-05	1.55E-08
7p	1.78E-02	3.04E-07	9.97E-04	4.09E-07	6.92E-05	1.07E-06	7.17E-06	5.51E-08
6d	1.83E-01	2.68E-07	8.83E-04	4.75E-07	2.89E-04	2.99E-06	3.19E-05	2.29E-07
6d	1.94E-01	3.63E-07	8.31E-04	1.92E-06	1.81E-04	2.26E-06	3.81E-05	1.37E-07
5f	1.99E-02	2.38E-07	1.05E-03	7.91E-08	2.60E-04	1.17E-06	9.20E-05	9.07E-08
5f	2.27E-02	2.36E-07	8.93E-04	7.19E-07	3.06E-04	4.88E-07	1.30E-04	6.20E-08
5g	7.07E-03	2.94E-09	2.59E-03	4.39E-06	4.98E-03	4.11E-06	3.18E-04	3.76E-07
5g	7.90E-03	2.06E-09	5.45E-03	4.60E-06	2.14E-03	7.15E-07	5.45E-05	5.56E-08
NORM-1 in case 95%								
7s	3.65E-01	-1.45E-06	-4.76E-03	-5.55E-06	-7.63E-05	-1.60E-05	9.20E-06	-7.06E-07
7p	1.79E-01	-5.42E-06	-8.38E-03	-3.17E-06	-8.29E-04	-8.94E-06	7.31E-05	4.21E-08
7p	1.89E-01	-2.05E-06	-6.57E-03	-3.26E-06	-5.06E-04	-8.06E-06	2.95E-05	3.04E-07
6d	1.83E+00	-9.93E-07	-4.95E-03	-3.05E-06	-1.37E-03	-1.78E-05	-1.47E-04	-1.26E-06
6d	1.46E+00	-1.42E-06	-2.16E-03	-9.17E-06	-8.14E-04	-1.10E-05	-1.35E-04	-5.60E-07
5f	4.72E-02	-1.85E-06	-6.49E-03	-3.34E-07	1.89E-03	-7.85E-06	6.27E-04	-5.76E-07
5f	3.05E-02	-1.54E-06	-4.18E-03	-3.97E-06	1.97E-03	-2.94E-06	8.32E-04	4.01E-07
5g	8.36E-01	9.30E-08	-3.50E-02	-1.34E-04	-2.75E-02	-1.08E-04	-4.02E-03	-9.23E-06
5g	8.22E-01	5.39E-08	-1.03E-02	-1.27E-04	-3.20E-02	-1.53E-05	-1.21E-03	-1.13E-06
SELF-CONSISTENCY in case 100%								
7s	2.06E-02	1.46E-07	3.39E-07	5.99E-08	3.10E-08	9.52E-09	7.99E-09	8.46E-09
7p	1.31E-02	1.21E-07	2.23E-07	3.39E-08	1.90E-08	6.53E-09	5.31E-09	5.26E-09
7p	1.97E-02	1.36E-07	7.69E-07	3.39E-08	1.83E-08	4.13E-09	1.90E-09	1.01E-09
6d	1.47E-01	1.37E-07	4.23E-07	1.59E-07	6.22E-08	9.39E-09	3.69E-09	1.69E-09
6d	1.68E-01	1.73E-07	5.19E-07	1.43E-07	5.62E-08	8.55E-09	3.20E-09	1.22E-09
5f	2.16E-02	4.63E-08	1.35E-06	7.82E-08	2.80E-08	3.64E-09	1.35E-09	5.35E-10
5f	2.40E-02	5.77E-08	1.61E-06	3.46E-08	1.42E-08	2.18E-09	8.58E-10	3.28E-10
5g	8.94E-03	4.19E-08	1.35E-04	2.45E-07	7.65E-08	7.04E-09	2.24E-09	7.69E-10
5g	9.77E-03	4.81E-08	8.24E-05	1.01E-07	2.93E-08	2.86E-09	9.56E-10	3.26E-10
NORM-1 in case 100%								
7s	3.77E-01	-1.69E-06	2.44E-06	-7.16E-07	-3.95E-07	-1.43E-07	-1.08E-07	-9.36E-08
7p	1.98E-01	-1.24E-06	-1.29E-06	-4.06E-07	-2.32E-07	-8.90E-08	-6.73E-08	-5.80E-08
7p	2.00E-01	-1.08E-06	-3.43E-06	-2.81E-07	-1.62E-07	-5.15E-08	-3.39E-08	-2.63E-08
6d	1.28E+00	-8.67E-07	-8.32E-07	-9.26E-07	-3.78E-07	-7.50E-08	-4.16E-08	-2.94E-08
6d	1.15E+00	-8.61E-07	-1.11E-06	-6.61E-07	-2.66E-07	-4.35E-08	-1.80E-08	-8.51E-09

Table 5. (Continued)

Subshell	1 var.		2 var.		3 var.		4 var.	
	In.	Fin.	In.	Fin.	In.	Fin.	In.	Fin.
5f	5.71E-02	-3.29E-07	-3.17E-06	-4.88E-07	-1.82E-07	-2.68E-08	-1.18E-08	-6.40E-09
5f	3.72E-02	-3.51E-07	-6.58E-06	-1.78E-07	-7.81E-08	-1.29E-08	-5.28E-09	-2.14E-09
5g	1.05E+00	-9.23E-07	-1.84E-03	-5.08E-06	-1.60E-06	-1.56E-07	-5.66E-08	-2.57E-08
5g	1.03E+00	-9.39E-07	-4.28E-04	-1.85E-06	-5.42E-07	-5.54E-08	-1.97E-08	-7.67E-09
SELF-CONSISTENCY in case regular								
7s	2.06E-02	1.45E-07						
7p ₋	1.31E-02	1.21E-07						
7p ₊	1.97E-02	1.36E-07						
6d	1.47E-01	1.36E-07						
6d ₋	1.68E-01	1.71E-07						
5f	2.16E-02	4.57E-08						
5f	2.40E-02	5.75E-08						
5g ₋	8.94E-03	3.86E-08						
5g	9.77E-03	4.67E-08						
NORM-1 in case regular								
7s	3.77E-01	-1.68E-06						
7p ₋	1.98E-01	-1.24E-06						
7p ₊	2.00E-01	-1.08E-06						
6d	1.28E+00	-8.57E-07						
6d ₋	1.15E+00	-8.54E-07						
5f	5.71E-02	-3.25E-07						
5f	3.72E-02	-3.50E-07						
5g ₋	1.05E+00	-8.35E-07						
5g	1.03E+00	-8.94E-07						

Table 6. SELF-CONSISTENCY and NORM-1 parameters solving the MCDHF equations of OS₂ for even parity states in 95, 99, 99.5, 99.95% and regular cases. Columns marked as in Table 4.

Subshell	1 var.		2 var.		3 var.		4 var.	
	In.	Fin.	In.	Fin.	In.	Fin.	In.	Fin.
SELF-CONSISTENCY in case 95%								
8s	1.30E-02	2.78E-06	1.44E-03	1.13E-06	1.10E-04	4.00E-07	1.98E-06	2.99E-07
8p ₋	2.00E-02	3.11E-06	4.88E-03	1.17E-06	1.37E-04	3.17E-07	3.15E-06	4.07E-07
8p ₊	2.34E-02	3.33E-06	4.32E-03	1.52E-06	1.81E-04	4.38E-07	8.81E-06	3.75E-07
7d ₋	1.62E-02	4.43E-06	1.92E-03	2.12E-06	2.47E-04	1.38E-06	8.28E-05	1.66E-06
7d ₊	2.00E-02	6.67E-06	2.54E-03	2.79E-06	2.10E-04	1.19E-06	1.11E-05	6.28E-07
6f	2.48E-02	7.65E-07	1.64E-03	1.54E-06	6.15E-04	6.54E-06	2.21E-04	9.37E-06
6f ₋	2.89E-02	1.99E-06	1.45E-03	3.01E-06	6.99E-04	1.09E-05	1.24E-04	6.61E-06
6g	2.53E-03	1.29E-08	7.80E-03	2.10E-08	8.40E-04	2.05E-07	1.14E-04	1.88E-07
6g ₋	2.90E-03	2.51E-08	9.87E-03	5.07E-08	1.14E-03	3.92E-07	6.57E-05	4.17E-07
NORM-1 in case 95%								
8s	2.77E+00	-1.82E-04	-6.46E-02	-7.35E-05	-7.06E-03	-2.54E-05	-1.11E-04	-1.88E-05
8p ₋	4.62E+00	-2.33E-04	-9.37E-03	-7.25E-05	-7.56E-03	5.53E-06	-1.91E-04	1.44E-05
8p ₊	3.89E+00	-1.59E-04	-4.01E-02	-5.88E-05	-6.25E-03	2.44E-06	-2.68E-04	6.65E-06
7d ₋	6.39E+00	-9.60E-05	-3.47E-02	-4.91E-05	-6.43E-03	-4.04E-05	-2.25E-03	-4.96E-05
7d ₊	6.49E+00	-1.14E-04	-3.47E-02	-5.31E-05	-1.96E-03	-2.61E-05	5.77E-07	-1.16E-05
6f	2.26E+00	-1.77E-05	-2.90E-02	-3.32E-05	-1.38E-02	-1.50E-04	-5.39E-03	-2.17E-04
6f ₋	2.24E+00	-3.83E-05	-2.40E-02	-5.83E-05	-1.41E-02	-2.23E-04	-2.47E-03	-1.36E-04
6g	2.32E+00	-6.24E-07	1.93E-01	-4.76E-07	-1.29E-02	-5.42E-06	-2.73E-03	-4.43E-06
6g ₋	2.34E+00	-1.90E-06	2.22E-01	-1.06E-06	-1.76E-02	-9.07E-06	-1.53E-03	-9.76E-06
SELF-CONSISTENCY in case 99.95%								
8s	1.27E-02	2.00E-06	6.35E-04	1.12E-07	7.33E-06	1.78E-07	2.02E-07	8.76E-08
8p ₋	4.49E-02	1.22E-06	1.37E-04	1.51E-07	7.95E-06	2.51E-07	2.77E-07	1.19E-07
8p ₊	4.23E-02	1.64E-06	1.68E-04	2.57E-07	5.89E-06	4.78E-07	4.48E-07	2.95E-07
7d ₋	1.78E-02	2.34E-06	2.53E-04	6.28E-07	4.24E-06	9.84E-07	8.12E-07	6.07E-07
7d ₊	2.18E-02	3.05E-06	2.10E-04	7.80E-07	5.18E-06	1.26E-06	9.68E-07	9.19E-07
6f	2.63E-02	1.21E-06	8.76E-04	3.36E-06	1.22E-05	4.67E-06	3.00E-06	2.41E-06
6f ₋	3.01E-02	1.52E-06	9.79E-04	3.93E-06	1.33E-05	5.62E-06	5.03E-06	3.84E-06
6g	8.88E-03	2.13E-07	1.49E-03	1.07E-05	1.40E-04	1.51E-05	2.23E-05	6.71E-06
6g ₋	1.00E-02	1.33E-07	1.56E-03	1.27E-05	1.76E-04	1.93E-05	5.99E-05	1.69E-05

Table 6. (Continued)

Subshell	1 var.		2 var.		3 var.		4 var.	
	In.	Fin.	In.	Fin.	In.	Fin.	In.	Fin.
NORM-1 in case 99.95%								
8s	2.71E+00	-8.54E-05	3.99E-03	2.44E-06	-2.48E-04	4.17E-06	3.15E-06	1.69E-06
8p ₋	1.22E+01	-6.57E-05	-3.70E-03	5.97E-06	3.09E-04	1.01E-05	1.31E-05	4.09E-06
8p ₊	6.02E+00	-5.35E-05	-5.57E-03	6.31E-06	1.78E-04	1.38E-05	1.61E-05	8.44E-06
7d ₋	7.52E+00	-5.59E-05	-6.65E-03	-1.27E-05	3.82E-05	-2.05E-05	-1.64E-05	-1.24E-05
7d ₊	7.70E+00	-5.93E-05	-1.83E-03	-1.24E-05	4.84E-05	-2.10E-05	-1.51E-05	-1.58E-05
6f ₋	2.29E+00	-2.60E-05	-1.81E-02	-7.60E-05	2.51E-06	-1.07E-04	-7.22E-05	-5.54E-05
6f ₊	2.26E+00	-2.86E-05	-1.78E-02	-7.78E-05	-1.59E-04	-1.12E-04	-1.03E-04	-7.69E-05
6g ₋	1.41E+00	1.02E-05	-5.35E-02	-8.23E-04	-1.10E-02	-1.22E-03	-1.30E-03	-5.44E-04
6g ₊	1.41E+00	5.52E-06	-5.17E-02	-8.79E-04	-1.25E-02	-1.41E-03	-3.49E-03	-1.26E-03
SELF-CONSISTENCY in case regular								
8s	1.28E-02	1.81E-07						
8p ₋	2.78E-02	2.98E-07						
8p ₊	5.61E-02	4.20E-07						
7d ₋	1.83E-02	9.36E-07						
7d ₊	2.22E-02	1.14E-06						
6f ₋	2.67E-02	4.32E-06						
6f ₊	3.06E-02	4.99E-06						
6g ₋	9.08E-03	1.41E-05						
6g ₊	1.01E-02	1.68E-05						
NORM-1 in case regular								
8s	2.72E+00	2.38E-06						
8p ₋	6.76E+00	1.29E-05						
8p ₊	8.44E+00	1.17E-05						
7d ₋	7.66E+00	-2.02E-05						
7d ₊	7.81E+00	-1.93E-05						
6f ₋	2.31E+00	-9.90E-05						
6f ₊	2.28E+00	-9.98E-05						
6g ₋	1.42E+00	-1.15E-03						
6g ₊	1.42E+00	-1.23E-03						

Table 7. SELF-CONSISTENCY and NORM-1 parameters solving the MCDHF equations of OS₂ for odd parity states in 95, 99.95% and regular cases. Columns marked as in Table 4.

Subshell	1 var.		2 var.		3 var.		4 var.	
	In.	Fin.	In.	Fin.	In.	Fin.	In.	Fin.
SELF-CONSISTENCY in case 95%								
8s	1.92E-02	4.01E-06	1.98E-03	1.43E-06	1.65E-04	7.28E-07	4.93E-06	1.19E-06
8p ₋	1.09E-02	2.59E-06	1.74E-03	2.10E-06	2.12E-04	9.39E-07	1.54E-05	1.40E-06
8p ₊	1.63E-02	3.55E-06	4.05E-03	3.37E-06	1.63E-02	1.58E-06	1.74E-05	2.05E-06
7d ₋	1.86E-02	6.64E-06	2.29E-03	3.25E-06	5.33E-03	1.77E-06	1.52E-04	5.03E-06
7d ₊	2.31E-02	9.54E-06	2.99E-03	4.47E-06	7.52E-03	2.28E-06	4.07E-05	2.44E-06
6f ₋	2.89E-02	2.02E-07	2.12E-03	4.43E-07	1.11E-04	3.54E-07	1.83E-05	7.14E-07
6f ₊	3.34E-02	8.92E-07	2.05E-03	1.36E-06	1.13E-04	5.80E-07	3.85E-05	1.74E-06
6g ₋	8.53E-03	6.13E-08	1.75E-03	3.53E-07	4.19E-04	6.46E-07	5.46E-05	2.85E-06
6g ₊	9.63E-03	8.86E-08	2.16E-03	8.10E-07	3.84E-04	7.26E-07	6.01E-05	2.01E-06
NORM-1 in case 95%								
8s	3.63E+00	-2.58E-04	-6.68E-02	-8.99E-05	-9.85E-03	-4.62E-05	-3.20E-04	-7.49E-05
8p ₋	5.19E+00	-1.85E-04	-5.97E-02	-1.29E-04	-1.11E-02	-5.63E-05	-8.60E-04	-8.37E-05
8p ₊	5.17E+00	-1.64E-04	-5.06E-02	-1.22E-04	2.82E-01	-5.97E-05	-5.73E-04	-7.13E-05
7d ₋	5.04E+00	-1.70E-04	-3.48E-02	-5.82E-05	5.12E-02	-3.62E-05	-2.90E-03	-1.24E-04
7d ₊	5.17E+00	-1.76E-04	-3.46E-02	-6.88E-05	6.55E-02	-3.72E-05	-6.31E-04	-3.74E-05
6f ₋	2.78E+00	-3.47E-06	-3.24E-02	-3.85E-06	6.74E-04	-4.65E-06	-2.17E-04	-1.03E-05
6f ₊	2.78E+00	-1.31E-05	-2.87E-02	-1.91E-05	-1.78E-03	-7.56E-06	-5.30E-04	-2.62E-05
6g ₋	1.97E+00	-3.76E-06	-6.62E-02	-1.78E-05	-2.31E-02	-3.69E-05	-3.58E-03	-1.70E-04
6g ₊	2.02E+00	-4.56E-06	-6.46E-02	-3.66E-05	-2.00E-02	-3.55E-05	-2.80E-03	-9.97E-05
SELF-CONSISTENCY in case 99.95%								
8s	1.53E-02	3.30E-06	2.55E-04	1.88E-07	1.35E-06	5.54E-07	3.44E-07	5.66E-08
8p ₋	1.20E-02	2.25E-06	2.44E-04	2.85E-07	8.84E-06	8.65E-07	4.29E-07	5.76E-08
8p ₊	1.71E-02	3.40E-06	2.40E-04	4.50E-07	4.45E-06	7.99E-07	6.02E-07	8.28E-08
7d ₋	1.92E-02	3.28E-06	2.99E-04	1.19E-06	2.30E-05	1.13E-06	6.49E-07	7.88E-08
7d ₊	2.35E-02	4.30E-06	3.41E-04	1.09E-06	1.65E-05	1.20E-06	7.19E-07	1.12E-07

Table 7. (Continued)

Subshell	1 var.		2 var.		3 var.		4 var.	
	In.	Fin.	In.	Fin.	In.	Fin.	In.	Fin.
6f	3.02E-02	3.54E-07	8.60E-04	8.35E-06	5.17E-06	1.75E-06	1.15E-06	2.96E-07
6f _̄	3.46E-02	4.51E-07	9.02E-04	8.88E-06	6.05E-06	1.27E-06	7.21E-07	1.47E-07
6g _̄	8.90E-03	1.26E-07	1.78E-03	9.31E-06	4.81E-05	8.40E-06	5.37E-06	9.23E-07
6g	1.01E-02	1.71E-07	1.79E-03	1.12E-05	1.04E-05	7.38E-07	2.53E-07	6.98E-08
NORM-1 in case 99.95%								
8s	2.66E+00	−1.18E-04	−6.42E-03	−8.82E-06	−5.44E-05	2.21E-05	1.43E-05	2.12E-06
8p _̄	5.34E+00	−1.11E-04	−9.91E-03	3.64E-06	4.06E-04	4.27E-05	2.14E-05	2.58E-06
8p	5.26E+00	−9.00E-05	−7.23E-03	6.23E-06	1.37E-04	2.18E-05	1.89E-05	2.33E-06
7d _̄	5.42E+00	−6.43E-05	−6.71E-03	−2.60E-05	3.43E-04	1.15E-05	4.94E-06	−9.51E-08
7d	5.48E+00	−6.98E-05	−1.51E-03	−1.64E-05	1.99E-04	1.11E-05	5.70E-06	7.73E-07
6f _̄	2.80E+00	−5.35E-07	−1.55E-02	−1.59E-04	−8.71E-05	−3.41E-05	−2.26E-05	−5.72E-06
6f	2.81E+00	−1.19E-06	−1.43E-02	−1.47E-04	−1.00E-04	−2.19E-05	−1.24E-05	−2.51E-06
6g _̄	2.03E+00	−6.29E-06	−6.56E-02	−5.26E-04	−2.78E-03	−4.85E-04	−3.20E-04	−5.34E-05
6g	2.07E+00	−7.34E-06	−6.15E-02	−5.68E-04	−1.41E-04	−3.83E-05	−1.41E-05	−3.59E-06
SELF-CONSISTENCY in case regular								
8s	1.52E-02	7.14E-05						
8p _̄	1.20E-02	2.44E-06						
8p	1.71E-02	3.49E-06						
7d _̄	1.91E-02	3.88E-06						
7d	2.34E-02	4.78E-06						
6f _̄	3.05E-02	5.63E-06						
6f	3.48E-02	6.17E-06						
6g _̄	9.44E-03	6.03E-06						
6g	1.05E-02	6.39E-06						
NORM-1 in case regular								
8s	2.65E+00	−1.51E-04						
8p _̄	5.37E+00	−1.20E-04						
8p	5.28E+00	−1.12E-04						
7d _̄	5.50E+00	−8.91E-05						
7d	5.55E+00	−8.59E-05						
6f _̄	2.80E+00	−1.05E-04						
6f	2.81E+00	−9.94E-05						
6g _̄	2.05E+00	−3.45E-04						
6g	2.12E+00	−3.23E-04						

Table 8 summarizes the CSF bases used in the MCDHF computations of OS_1 and OS_2 . The number of CSFs is given for each variation step using the RSMBPT method with a different fraction, as well as in the regular GRASP2018 calculations. It is seen that the largest change in the number of CSFs occurs after the first variation when the selection procedure is based on radial wavefunctions estimated using the Thomas–Fermi potential. After a few variations, the CSF basis almost does not change.

Table 8. Number of CSF in the MCDHF computations of OS_1 and OS_2 using the regular way and the RSMBPT method.

Case	OS_1				OS_2			
	1 var.	2 var.	3 var.	4 var.	1 var.	2 var.	3 var.	4 var.
Even								
95%	508364	569574	570467	571019	733794	1023336	1141939	1147646
99%	689625	785778	898767	897052	1194590	1746407	1806590	1847202
99.5%	772411	880322	980963	981664	1398101	1979519	2071879	2111506
99.95%	966043	1144631	1173196	1173442	1944852	2525688	2567785	2567315
100%	1287673	1303671	1303659	1303659				
Regular	1303709				2923523			
Odd								
95%	197074	226517	245285	248960	280434	422802	439826	442597
99%	269522	322049	340528	340543	465186	685001	700179	700938
99.5%	303520	353355	371760	371834	550123	783504	799867	799302
99.95%	380829	444754	450637	450656	764152	973620	974618	974715
100%	500591	507233	507231	507231				
Regular	507234				1126622			

Table 9 presents the total energies from the regular **CV+C+VV MCDHF** and the differences between the **CV+C+VV MCDHF (RSMBPT 95%)** and **CV+C+VV MCDHF** calculations. In the last lines of the table, the smallest (ΔE_{\min}) and the largest (ΔE_{\max}) differences with the results of the regular GRASP2018 calculations (**CV+C+VV MCDHF**), as well as the root-mean-square (rms), are given for each computation. This table shows the results for all computed even states of OS_1 .

As seen from the table, the results converge and almost do not change after few variations. The differences between both (regular and RSMBPT 95%) computations are similar for most levels at the same variation. The rms in the 'case 95%' is equal to 0.00847 a.u. at the final variation step, the ΔE_{\min} is 0.00586 a.u. (or 0.00024%) and ΔE_{\max} is 0.01143 a.u. (or 0.00047%).

Since the trends are similar, only a summary of the ΔE_{\min} , ΔE_{\max} and rms is presented in Table 10

for the remaining computed cases. It is seen that by including the most significant CV+C+VV correlations – increasing the amount of these correlations (95, 99, 99.5, 99.95 and 100%) – the results converge to the regular GRASP2018 results, and in the case of '100%', reproduce them.

Furthermore, the results with the specified amount (95, 99, 99.5, 99.95%) of correlations also show good agreement with the regular GRASP2018 data, but the CSF bases are significantly smaller compared to the regular ones, and this is relevant for complex systems when CSF bases grow rapidly with each new OS and each opened core shell. It should be noted that in some cases, especially when the specified fraction of correlations is smaller, the order of levels that are very close to each other can differ from the regular computations.

Based on the results of the above investigations, it can be concluded that the RSMBPT method can be successfully applied to solve the self-consistent

Table 9. The total energies (in a.u.) from **CV+C+VV MCDHF** calculations and differences (in a.u.) between **CV+C+VV MCDHF (RSMBPT 95%)** and **CV+C+VV MCDHF** energies ($\Delta E_{(\text{CV+C+VV MCDHF (RSMBPT 95\%)} - (\text{CV+C+VV MCDHF}))}$) for the OS_1 even states of Se III are given when CV, C and VV correlations are included in the computations. 'Pos' means numbering of the levels for specific parity and J value in the spectra. 'Pos' means numbering of the levels for specific parity and J value in the spectra.

No	Pos	J	CV+C+VV MCDHF	$\Delta E_{(\text{CV+C+VV MCDHF (RSMBPT 95\%)} - (\text{CV+C+VV MCDHF}))}$			
				1 var.	2 var.	3 var.	4 var.
1	1	0	-2427.69766	0.01720	0.01069	0.01064	0.01063
2	1	1	-2427.68992	0.01376	0.00967	0.00965	0.00965
3	1	2	-2427.67956	0.01392	0.00928	0.00929	0.00925
4	2	2	-2427.62985	0.01449	0.00987	0.00988	0.00982
5	2	0	-2427.55745	0.01781	0.01153	0.01143	0.01143
6	2	1	-2427.01492	0.01389	0.00996	0.00988	0.00990
7	3	1	-2427.00375	0.01349	0.00948	0.00940	0.00941
8	3	2	-2427.00215	0.01374	0.00942	0.00938	0.00938
9	3	0	-2426.99672	0.01417	0.00981	0.00978	0.00978
10	4	1	-2426.98955	0.01317	0.00942	0.00940	0.00940
11	1	3	-2426.98713	0.01389	0.01011	0.01011	0.01009
12	4	2	-2426.98275	0.01314	0.00937	0.00939	0.00938
13	5	1	-2426.97557	0.01318	0.00960	0.00961	0.00961
14	5	2	-2426.96569	0.01317	0.00948	0.00948	0.00947
15	4	0	-2426.93852	0.01453	0.01000	0.00995	0.00998
16	2	3	-2426.83386	0.01186	0.00832	0.00821	0.00826
17	3	3	-2426.83285	0.01175	0.00816	0.00804	0.00806
18	6	2	-2426.83227	0.01176	0.00828	0.00823	0.00823
19	1	4	-2426.83154	0.01181	0.00804	0.00795	0.00794
20	4	3	-2426.81616	0.01089	0.00811	0.00812	0.00812
21	2	4	-2426.81479	0.01092	0.00801	0.00796	0.00796
22	1	5	-2426.81101	0.01158	0.00834	0.00836	0.00836
23	5	3	-2426.81033	0.01087	0.00801	0.00803	0.00803
24	7	2	-2426.81002	0.01143	0.00789	0.00790	0.00789
25	8	2	-2426.80844	0.01203	0.00791	0.00795	0.00794
26	6	1	-2426.80686	0.01211	0.00898	0.00897	0.00897
27	3	4	-2426.80572	0.01076	0.00789	0.00789	0.00789

Table 9. (Continued)

No	Pos	J	CV+C+VV MCDHF	$\Delta E_{(CV+C+VV \text{ MCDHF (RSMBPT 95\%)})-(CV+C+VV \text{ MCDHF})}$			
				1 var.	2 var.	3 var.	4 var.
28	7	1	–2426.80439	0.01323	0.00884	0.00879	0.00879
29	9	2	–2426.80383	0.01119	0.00828	0.00831	0.00831
30	8	1	–2426.80260	0.01277	0.00797	0.00798	0.00798
31	5	0	–2426.80242	0.01371	0.00916	0.00911	0.00912
32	9	1	–2426.80136	0.01186	0.00802	0.00798	0.00798
33	10	2	–2426.79932	0.01146	0.00661	0.00660	0.00659
34	11	2	–2426.79862	0.01317	0.00918	0.00918	0.00918
35	10	1	–2426.79633	0.01297	0.00863	0.00724	0.00859
36	6	3	–2426.79576	0.01180	0.00671	0.00802	0.00668
37	6	0	–2426.79175	0.01333	0.00870	0.00868	0.00868
38	4	4	–2426.79069	0.01191	0.00686	0.00682	0.00680
39	11	1	–2426.78465	0.01285	0.00947	0.00942	0.00938
40	2	5	–2426.78375	0.01248	0.00707	0.00710	0.00711
41	12	2	–2426.78245	0.01310	0.00953	0.00948	0.00950
42	7	3	–2426.78179	0.01322	0.00997	0.00998	0.00997
43	12	1	–2426.77863	0.01289	0.00954	0.00949	0.00944
44	13	2	–2426.77630	0.01292	0.00948	0.00945	0.00944
45	13	1	–2426.77491	0.01309	0.00774	0.00771	0.00771
46	7	0	–2426.77373	0.01223	0.00760	0.00762	0.00761
47	14	1	–2426.77325	0.01326	0.00733	0.00732	0.00731
48	14	2	–2426.77270	0.01185	0.00720	0.00720	0.00719
49	8	3	–2426.77095	0.01267	0.00747	0.00745	0.00745
50	5	4	–2426.76765	0.01243	0.00764	0.00762	0.00760
51	15	2	–2426.76742	0.01176	0.00750	0.00746	0.00747
52	8	0	–2426.76382	0.01384	0.00995	0.00992	0.00990
53	9	3	–2426.75799	0.01235	0.00773	0.00773	0.00773
54	16	2	–2426.75562	0.01261	0.00805	0.00801	0.00799
55	9	0	–2426.73726	0.01430	0.00817	0.00816	0.00816
56	17	2	–2426.73526	0.01045	0.00590	0.00589	0.00586
57	15	1	–2426.73136	0.01341	0.00763	0.00758	0.00758
58	10	3	–2426.72985	0.01039	0.00617	0.00614	0.00613
59	11	3	–2426.72832	0.01190	0.00706	0.00704	0.00704
60	18	2	–2426.72492	0.01117	0.00670	0.00670	0.00669
61	16	1	–2426.72245	0.01133	0.00678	0.00679	0.00679
62	6	4	–2426.72195	0.01087	0.00639	0.00637	0.00634
63	19	2	–2426.72081	0.01223	0.00756	0.00753	0.00753
ΔE_{\min} (in a.u.)				0.01039	0.00590	0.00589	0.00586
ΔE_{\max} (in a.u.)				0.01781	0.01153	0.01143	0.01143
rms (in a.u.)				0.01274	0.00850	0.00848	0.00847

field equations. Using this method, the most important chosen correlations with the specified fraction can be selected, since to include different types of correlations in the MCDHF calculations in the regular way is often a complex task, especially for complex systems. The radial wavefunctions (obtained using the RSMBPT method) which themselves include the most significant correlations can be used for further RCI calculations.

5.2.2. Results from RCI calculations

Tables 11 and 12 present the results of the RCI computations. As it was described above (see Section 5.1), the RCI computations were performed in the regular way and using two different procedures within the framework of RSMBPT method. In the first procedure using the RSMBPT method, the radial wavefunctions were taken from

Table 10. The smallest (ΔE_{\min} in a.u.) and the largest (ΔE_{\max} in a.u.) differences and rms of total energies from the MCDHF computations of OS_1 and OS_2 comparing the results from the regular way and the RSMBPT method.

	Even				Odd			
	1 var.	2 var.	3 var.	4 var.	1 var.	2 var.	3 var.	4 var.
OS_1								
Case 95%								
ΔE_{\min} (in a.u.)	0.01039475	0.00589933	0.00588704	0.00586482	0.01078587	0.00619445	0.00410314	0.00378723
ΔE_{\max} (in a.u.)	0.01781291	0.01153240	0.01143447	0.01143258	0.01615159	0.00844032	0.00543860	0.00506363
rms (in a.u.)	0.01274465	0.00850122	0.00847525	0.00847151	0.01345016	0.00724574	0.00455746	0.00430101
Case 99%								
ΔE_{\min} (in a.u.)	0.00479198	0.00241481	0.00044516	0.00044752	0.00444358	0.00147206	0.00072496	0.00072521
ΔE_{\max} (in a.u.)	0.01010324	0.00488030	0.00122598	0.00123373	0.00864969	0.00231023	0.00107323	0.00105647
rms (in a.u.)	0.00692783	0.00366682	0.00081360	0.00081380	0.00723871	0.00182232	0.00086627	0.00086609
Case 99.5%								
ΔE_{\min} (in a.u.)	0.00403621	0.00124726	0.00022377	0.00022392	0.00322708	0.00075465	0.00036678	0.00035865
ΔE_{\max} (in a.u.)	0.00892285	0.00265308	0.00078628	0.00078657	0.00729924	0.00126755	0.00055566	0.00054793
rms (in a.u.)	0.00591419	0.00182666	0.00046031	0.00045983	0.00602911	0.00094146	0.00044813	0.00044605
Case 99.95%								
ΔE_{\min} (in a.u.)	0.00248536	0.00011430	0.00002831	0.00002734	0.00352790	0.00005336	0.00003057	0.00003065
ΔE_{\max} (in a.u.)	0.00591823	0.00032153	0.00017859	0.00017856	0.00581758	0.00013347	0.00007381	0.00007382
rms (in a.u.)	0.00422965	0.00021375	0.00007648	0.00007318	0.00479534	0.00009420	0.00005156	0.00005162
Case 100%								
ΔE_{\min} (in a.u.)	0.00003567	0.00000000	0.00000000	0.00000000	0.00003871	0.00000000	0.00000000	0.00000000
ΔE_{\max} (in a.u.)	0.00008260	0.00000078	0.00000078	0.00000078	0.00007884	0.00000001	0.00000003	0.00000003
rms (in a.u.)	0.00006240	0.00000015	0.00000015	0.00000015	0.00006174	0.00000001	0.00000001	0.00000001
OS_2								
Case 95%								
ΔE_{\min} (in a.u.)	0.01514835	0.00565667	0.00465128	0.00476963	0.01905315	0.00664994	0.00635027	0.00628709
ΔE_{\max} (in a.u.)	0.02611409	0.01186351	0.00944572	0.00948070	0.02458143	0.00895267	0.00824978	0.00825399
rms (in a.u.)	0.01959744	0.00889209	0.00680218	0.00676645	0.02082576	0.00747281	0.00703090	0.00698012
Case 99%								
ΔE_{\min} (in a.u.)	0.00879110	0.00085163	0.00081118	0.00076419	0.01077293	0.00157237	0.00150440	0.00150264
ΔE_{\max} (in a.u.)	0.01554800	0.00279595	0.00235952	0.00232113	0.01502497	0.00238582	0.00228452	0.00228469
rms (in a.u.)	0.01167577	0.00205255	0.00177316	0.00168195	0.01235068	0.00183188	0.00177058	0.00177014
Case 99.5%								
ΔE_{\min} (in a.u.)	0.00770291	0.00034064	0.00041791	0.00041622	0.00862058	0.00093582	0.00081631	0.00081282
ΔE_{\max} (in a.u.)	0.01361750	0.00188676	0.00154804	0.00153272	0.01279172	0.00150648	0.00140862	0.00140949
rms (in a.u.)	0.00996782	0.00133000	0.00107452	0.00101776	0.01058859	0.00111489	0.00104843	0.00104674
Case 99.95%								
ΔE_{\min} (in a.u.)	0.00388888	0.00005463	0.00007514	0.00007001	0.00450417	0.00014034	0.00012899	0.00012840
ΔE_{\max} (in a.u.)	0.00911764	0.00047941	0.00040230	0.00040681	0.00806687	0.00040195	0.00038392	0.00038297
rms (in a.u.)	0.00571790	0.00033027	0.00026441	0.00026029	0.00624877	0.00024094	0.00026036	0.00026023

the **CV+C+VV MCDHF (RSMBPT)** calculations and the CSF basis was taken from the regular GRASP2018 calculations. In the second procedure, the radial wavefunctions were taken from the **CV+C+VV MCDHF (RSMBPT)** calculations and the CSF basis was constructed using the RSMBPT method with the same specified fraction as in the MCDHF.

Table 11 presents the summary of rms, of the smallest (ΔE_{\min}) and the largest (ΔE_{\max}) dif-

ferences comparing the total energies from the **CV+C+VV RCI (RSMBPT)** method with the regular GRASP2018 calculations (**CV+C+VV RCI**). As seen from the table, the results (these in columns 2 and 4) from the first procedure using the RSMBPT method in the case of ‘100%’ reproduce the results from the regular calculations. Using the radial wavefunctions from the **CV+C+VV MCDHF (RSMBPT)** calculations with a decreased amount of these correlations (99.95, 99.5, 99, 95%),

Table 11. The smallest (ΔE_{\min} in a.u.) and the largest (ΔE_{\max} in a.u.) differences and rms of total energies from the RCI computations of OS_1 and OS_2 comparing the results from the regular way and using the RSMBPT method.

	Even		Odd	
	First procedure	Second procedure	First procedure	Second procedure
OS_1				
Radial wavefunctions from case 95%				
ΔE_{\min} (in a.u.)	0.00304085		0.00000286	
ΔE_{\max} (in a.u.)	0.00769594		0.00009646	
rms (in a.u.)	0.00494324		0.00004479	
Radial wavefunctions from case 99%				
ΔE_{\min} (in a.u.)	0.00000019		0.00000016	
ΔE_{\max} (in a.u.)	0.00001724		0.00001468	
rms (in a.u.)	0.00000680		0.00000555	
Radial wavefunctions from case 99.5%				
ΔE_{\min} (in a.u.)	0.00000001		0.00000034	
ΔE_{\max} (in a.u.)	0.00001541		0.00001237	
rms (in a.u.)	0.00000398		0.00000637	
Radial wavefunctions from case 99.95%				
ΔE_{\min} (in a.u.)	0.00000002		0.00000003	
ΔE_{\max} (in a.u.)	0.00000178		0.00000189	
rms (in a.u.)	0.00000074		0.00000083	
Radial wavefunctions from case 100%				
ΔE_{\min} (in a.u.)	0.00000000		0.00000000	
ΔE_{\max} (in a.u.)	0.00000006		0.00000003	
rms (in a.u.)	0.00000003		0.00000001	
OS_2				
Radial wavefunctions from case 95%				
ΔE_{\min} (in a.u.)	0.00005090	0.00478032	0.00004574	0.00630025
ΔE_{\max} (in a.u.)	0.00197267	0.00952692	0.00094435	0.00826736
rms (in a.u.)	0.00098455	0.00678775	0.00043676	0.00698827
Radial wavefunctions from case 99%				
ΔE_{\min} (in a.u.)	0.00000458	0.00074870	0.00000710	0.00151110
ΔE_{\max} (in a.u.)	0.00023362	0.00232700	0.00029347	0.00229393
rms (in a.u.)	0.00014306	0.00167533	0.00009579	0.00177984
Radial wavefunctions from case 99.5%				
ΔE_{\min} (in a.u.)	0.00000024	0.00041214	0.00000244	0.00081798
ΔE_{\max} (in a.u.)	0.00008720	0.00154291	0.00014983	0.00141603
rms (in a.u.)	0.00004940	0.00102058	0.00004814	0.00105443
Radial wavefunctions from case 99.95%				
ΔE_{\min} (in a.u.)	0.00000018	0.00007105	0.00000004	0.00012925
ΔE_{\max} (in a.u.)	0.00002741	0.00041042	0.00001590	0.00038453
rms (in a.u.)	0.00000952	0.00026222	0.00000824	0.00026121

the differences increase, but the results are still in good agreement with the regular calculations.

In the second procedure, when the RSMBPT method is applied to obtain the radial wavefunctions and the CSF basis (results in columns 3 and 5), the differences between the two calculations are even larger. The rms in the case when 95% of the CV, C and VV correlations are included in both (MCDHF and RCI) computations, is equal

to 0.00678775 a.u. and ΔE_{\max} for this computation is equal to 0.00952692 a.u. (or 0.00039276%). By increasing the amount of these correlations the differences decrease, and in the case when 99.95% of the CV, C and VV correlations are included in both (MCDHF and RCI) computations, the rms is equal to 0.00026222 a.u. and ΔE_{\max} for this computation is equal to 0.00041042 a.u. (or 0.00001693%).

Table 12. Energy levels (in cm^{-1}) from **CV+C+VV RCI** calculations and differences (in cm^{-1}) between **CV+C+VV RCI (RSMBPT)** and **CV+C+VV RCI** energies ($\Delta E_{(\text{CV+C+VV RCI (RSMBPT)})-(\text{CV+C+VV RCI})}$) for the OS_2 even states of Se III are given when CV, C and VV correlations are included in the computations.

No	Pos	J	CV+C+VV RCI	$\Delta E_{(\text{CV+C+VV RCI (RSMBPT)})-(\text{CV+C+VV RCI})}$			
				First procedure		Second procedure	
				95%	99.95%	95%	99.95%
1	1	0	0.00	0.00	0.00	0.00	0.00
2	1	1	1682.62	3.75	-0.32	-330.09	-21.68
3	1	2	3889.34	6.04	-0.88	-411.08	-24.74
4	2	2	13797.80	23.17	1.86	-312.40	-20.79
5	2	0	29482.86	82.02	2.96	152.76	-4.49
6	2	1	151160.29	-98.23	-3.90	-257.70	27.52
7	3	1	153592.00	-99.55	-2.97	-330.38	25.41
8	3	2	153914.82	-102.93	-3.31	-325.03	25.14
9	3	0	155152.31	-89.78	-1.29	-193.47	34.01
10	4	1	156676.51	-91.53	-2.96	-341.68	26.93
11	1	3	157184.53	-103.16	-4.01	-140.65	35.61
12	4	2	158137.34	-89.27	-3.00	-322.07	27.12
13	5	1	159722.61	-95.52	-3.69	-354.90	26.77
14	5	2	161643.32	-86.43	-2.54	-314.04	26.27
15	4	0	167467.38	-75.92	-3.37	-122.41	27.77
16	2	3	191065.56	-528.12	-0.05	-485.28	43.60
17	3	3	191311.15	-529.97	1.45	-514.99	41.16
18	6	2	191438.47	-548.76	-0.15	-507.27	45.48
19	1	4	191591.48	-539.72	1.80	-517.79	40.19
20	4	3	194890.31	-530.86	-1.54	-551.92	41.63
21	7	2	195071.18	-165.89	0.05	-521.09	-10.96
22	2	4	195200.75	-530.91	-0.13	-546.13	39.68
23	1	5	196006.00	-515.51	0.22	-393.95	49.73
24	5	3	196208.59	-536.94	0.38	-561.74	40.04
25	8	2	196466.68	-548.38	-1.25	-570.10	43.26
26	6	1	196813.18	-252.84	-0.55	-503.12	0.60
27	7	1	197037.20	-284.25	-2.11	-540.48	35.23
28	3	4	197214.70	-598.63	-0.45	-518.21	47.03
29	8	1	197246.38	-290.55	-0.44	-544.53	-10.35
30	5	0	197413.53	-119.00	-0.72	-335.69	7.73
31	9	2	197572.23	-505.66	0.61	-759.66	24.24
32	10	2	197711.31	-314.91	0.10	-526.22	4.17
33	9	1	197869.14	-249.40	-2.31	-296.61	40.00
34	6	3	198439.99	-280.51	0.28	-741.17	-12.80
35	10	1	198691.21	-122.59	-1.98	-323.69	18.69
36	11	2	198745.26	-161.50	-2.13	-319.87	29.04
37	6	0	199454.22	-118.96	-1.28	-229.36	24.29
38	4	4	199536.16	-265.27	0.51	-655.89	-8.93
39	2	5	201028.11	-254.34	0.55	-510.49	5.09
40	11	1	201813.06	-100.54	-4.12	-318.12	31.11
41	12	2	202295.91	-102.62	-4.02	-253.44	32.55
42	7	3	202470.62	-103.20	-3.94	-152.60	34.19
43	12	1	203148.82	-105.64	-3.87	-546.49	30.00
44	7	0	203351.47	-215.51	-0.54	-610.10	-12.55
45	13	1	203404.08	-206.94	-0.46	-552.38	-15.50
46	13	2	203527.76	-181.36	-1.88	-766.05	1.90
47	14	2	203618.74	-137.47	-1.61	-322.28	10.36
48	8	3	203950.72	-203.44	0.25	-665.57	-12.78
49	14	1	204211.81	-110.85	-0.82	-593.82	-16.51
50	5	4	204652.02	-190.72	0.44	-547.98	-6.71
51	15	2	205754.78	-110.57	-1.17	-678.00	-16.14
52	8	0	206137.41	-88.19	-4.35	-133.73	29.68
53	16	2	206141.26	-139.46	1.66	-386.88	1.47
54	9	3	207759.36	-115.37	-1.37	-591.68	-11.84
55	17	2	211050.37	-339.75	5.05	-888.99	0.95
56	9	0	212148.21	-122.03	-4.03	-457.05	-12.15
57	10	3	212253.84	-336.77	3.95	-783.63	7.51
58	11	3	213384.11	-189.00	1.09	-690.00	-14.25
59	15	1	213402.16	-123.00	-3.91	-636.39	-14.85
60	6	4	213959.74	-332.19	2.60	-651.72	11.21
61	18	2	214098.17	-219.75	-0.92	-870.78	-19.97
62	16	1	214627.71	-237.65	-2.08	-854.12	-20.46
63	19	2	215656.63	-125.53	-3.35	-658.07	-14.78
N_{CSFs}				2923523	2923523	1148711	2567016
rms (in cm^{-1})				276.96	2.32	509.08	25.92

Table 12 shows the comparison of energy levels from the regular GRASP2018 calculations and the calculations using the RSMBPT method for the OS_2 even states. In the Table, energy levels from the regular calculations and the differences between the **CV+C+VV RCI (RSMBPT)** and **CV+C+VV RCI** calculations are given. The results of the **CV+C+VV RCI (RSMBPT)** calculations are given only for two boundary cases (when radial wavefunctions are taken from the **CV+C+VV MCDHF (RSMBPT)** calculations in two cases, 99.95 and 95%). The rms deviations obtained for the first procedure RCI calculations from the regular GRASP2018 data are 276.96 and 2.32 cm^{-1} , respectively, when 95 or 99.95% of the CV, C and VV correlations are included in the MCDHF. It should be noted that the energies of the computed states are up to 216000 cm^{-1} . The differences increase when the RSMBPT method is used for the MCDHF and RCI computations (the second procedure). In this procedure, the rms deviations from the regular GRASP2018 data are 509.08 and 25.92 cm^{-1} , respectively, when 95 or 99.95% of the CV, C and VV correlations are included in both (MCDHF and RCI) computations. The largest difference between the regular calculations and calculations when 95% of the CV, C and VV correlations are included in both (MCDHF and RCI) computations is equal to 888.99 cm^{-1} (or 0.421%), and in the case of 99.95% it is equal to 49.73 cm^{-1} (or 0.025%).

6. Conclusions

The method, based on the Rayleigh–Schrödinger perturbation theory in an irreducible tensorial form, is extended to estimate the valence–valence correlations, which are described by the three-particle Feynman diagram. The expressions to calculate the influence of these correlations are provided, also additional developments to calculate the spin-angular parts of the three-particle Feynman diagram have been made to the program library `librang` of the GRASP. This extended RSMBPT method allows one to estimate the contribution of any K' configuration of the CV, C, CC and VV correlations with a preferred core, virtual orbitals sets, and with any number of valence electrons for any atom or ion.

This is the first time that CSF bases constructed using the RSMBPT method have been used to solve

the self-consistent field equations. Previously, this method was only applied to RCI computations. Thus, this work demonstrates the third way of the application of the RSMBPT method in atomic calculations (other two ways of its application are presented in a series of previous papers by G. Gaigalas, P. Rynkun, and L. Kitovienė).

The use of the RSMBPT method in the MCDHF computations enables the inclusion of the most significant correlations of various types, which is not very feasible in regular GRASP calculations, especially for complex systems. Based on the results obtained in this study work, it can be concluded that the RSMBPT method can be successfully applied to solve the self-consistent field equations.

The radial wavefunctions obtained using the RSMBPT method can be used in the RCI computations in several procedures: i) these can be used with the extended CSF basis; or ii) these can be used with the CSF basis constructed using the RSMBPT method with the specified fraction as in the MCDHF. The results of both RCI computations are in good agreement with the results of the regular RCI computations.

References

- [1] G. Gaigalas, P. Rynkun, and L. Kitovienė, Second-order Rayleigh–Schrödinger perturbation theory for the GRASP2018 package: Core–valence correlations, *Lith. J. Phys.* **64**(1), 20–39 (2024), <https://doi.org/10.3952/physics.2024.64.1.3>
- [2] G. Gaigalas, P. Rynkun, and L. Kitovienė, Second-order Rayleigh–Schrödinger perturbation theory for the GRASP2018 package: Core correlations, *Lith. J. Phys.* **64**(2), 73–81 (2024), <https://doi.org/10.3952/physics.2024.64.2.1>
- [3] G. Gaigalas, P. Rynkun, and L. Kitovienė, Second-order Rayleigh–Schrödinger perturbation theory for the GRASP2018 package: Core–core correlations, *Lith. J. Phys.* **64**(3), 139–161 (2024), <https://doi.org/10.3952/physics.2024.64.3.1>
- [4] G. Gaigalas, P. Rynkun, and L. Kitovienė, Second-order Rayleigh–Schrödinger perturbation theory for the GRASP2018 package: Valence–valence correlations, *Lith. J. Phys.* **65**(1), 32–56 (2025), <https://doi.org/10.3952/physics.2025.65.1.2>
- [5] C. Froese Fischer, G. Gaigalas, P. Jönsson, and J. Bieroń, GRASP2018—A Fortran 95 version of the

- General Relativistic Atomic Structure Package, *Comput. Phys. Commun.* **237**, 184–187 (2019), <https://doi.org/10.1016/j.cpc.2018.10.032>
- [6] C. Froese Fischer, M. Godefroid, T. Brage, P. Jönsson, and G. Gaigalas, Advanced multiconfiguration methods for complex atoms: I. Energies and wave functions, *J. Phys. B* **49**(18), 182004 (2016), <https://doi.org/10.1088/0953-4075/49/18/182004>
- [7] P. Jönsson, M. Godefroid, G. Gaigalas, J. Ekman, J. Grumer, W. Li, J. Li, T. Brage, I.P. Grant, J. Bieroń, and C. Froese Fischer, An introduction to relativistic theory as implemented in GRASP, *Atoms* **11**(7), 1 (2023), <https://doi.org/10.3390/atoms11010007>
- [8] I. Lindgren and J. Morrison, *Atomic Many-body Theory* (Springer-Verlag Berlin Heidelberg, New York, 1982).
- [9] G. Gaigalas, A program library for computing pure spin-angular coefficients for one- and two-particle operators in relativistic atomic theory, *Atoms* **10**(4), 129 (2022), <https://doi.org/10.3390/atoms10040129>
- [10] G. Gaigalas and Z. Rudzikas, On the secondly quantized theory of the many-electron atom, *J. Phys. B* **29**(15), 3303 (1996), <https://doi.org/10.1088/0953-4075/29/15/007>
- [11] G. Gaigalas, Z. Rudzikas, and C. Froese Fischer, An efficient approach for spin-angular integrations in atomic structure calculations, *J. Phys. B* **30**(17), 3747 (1997), <https://doi.org/10.1088/0953-4075/30/17/006>
- [12] G. Gaigalas, *Irreducible Tensorial Form of the Stationary Perturbation Theory for Atoms and Ions with Open Shells*, PhD Thesis (Institute of Physics, Vilnius, 1989), <https://kolekcijos.biblioteka.vu.lt/en/objects/990007058341008452#00001> [in Russian].
- [13] G. Gaigalas, J. Kaniauskas, and Z. Rudzikas, Diagrammatic technique of the angular momentum theory and second quantization, *Liet. Fiz. Rink. (Sov. Phys. Coll.)* **25**, 3–13 (1985) [in Russian].
- [14] A.P. Jucys and A.A. Bandzaitis, *Theory of Angular Momentum in Quantum Mechanics* (Mokslas, Vilnius, 1977) [in Russian].
- [15] A.P. Yutsis, J.B. Levinson, and V.V. Vanagas, *Mathematical Apparatus of the Theory of Angular Momentum* (Israel Program for Scientific Translations Ltd, 1962).
- [16] D.M. Brink and G.R. Satchler, *Angular Momentum* (Clarendon Press, Oxford, 1968).
- [17] E. El Blaz, B. Castel, *Graphical Methods of Spin Algebra in Atomic, Nuclear, and Particle Physics* (Marcel Dekker, New York, 1972).
- [18] D.A. Varshalovich, A.N. Moskalev, and V.K. Khersonskii, *Quantum Theory of Angular Momentum* (World Scientific, Singapore, New Jersey, Hong Kong, 2021).
- [19] Y.T. Li, K. Wang, R. Si, M. Godefroid, G. Gaigalas, Ch.Y. Chen, and P. Jönsson, Reducing the computational load – atomic multiconfiguration calculations based on configuration state function generators, *Comput. Phys. Commun.* **283**, 108562 (2023), <https://doi.org/10.1016/j.cpc.2022.108562>
- [20] R. Si, Y. Li, K. Wang, Ch. Chen, G. Gaigalas, M. Godefroid, and P. Jönsson, GRASPG – An extension to GRASP2018 based on configuration state function generators, *Comput. Phys. Commun.* **312**, 109604 (2025), <https://doi.org/10.1016/j.cpc.2025.109604>
- [21] K. Dyall, I. Grant, C. Johnson, F. Parpia, and E. Plummer, GRASP: A general-purpose relativistic atomic structure program, *Comput. Phys. Commun.* **55**, 425 (1989), [https://doi.org/10.1016/0010-4655\(89\)90136-7](https://doi.org/10.1016/0010-4655(89)90136-7)
- [22] G. Gaigalas, P. Rynkun, N. Domoto, M. Tanaka, D. Kato, and L. Kitovienė, Theoretical investigation of energy levels and transitions for Ce III with applications to kilonova spectra, *MNRAS* **530**, 5220 (2024), <https://doi.org/10.1093/mnras/stae1196>
- [23] P. Jönsson, G. Gaigalas, C. Froese Fischer, J. Bieroń, I.P. Grant, T. Brage, J. Ekman, M. Godefroid, J. Grumer, J. Li, and W. Li, GRASP manual for users, *Atoms* **11**, 68 (2023), <https://doi.org/10.3390/atoms11040068>

ANTROSIOS EILĖS RELĖJAUS IR ŠRĖDINGERIO TRIKDYMŲ TEORIJA GRASP2018 PROGRAMINIAM PAKETUI: TRIJŲ DALELIŲ FEINMANO DIAGRAMOS ĮTAKA VALENTINĖMS–VALENTINĖMS KORELIACIJOMS*

G. Gaigalas, P. Rynkun, L. Kitovienė

Vilniaus universiteto Fizikos fakulteto Teorinės fizikos ir astronomijos institutas, Vilnius, Lietuva

Santrauka

Antrosios eilės trikdymų teorija paremtas metodas, skirtas įvairių koreliacijų vertei nustatyti, išplėstas įtraukiant valentines–valentines koreliacijas, kurios aprašomos trijų dalelių Feinmano diagrama. Šis išplėtimas papildo kamieno–valentines, kamieno, kamieno–kamieno ir valentines–valentines koreliacijas, kurios buvo išplėtos ankstesniuose G. Gaigalo, P. Rynkuno ir L. Kitovienės darbuose. Kadangi šios valentinės–valentinės koreliacijos yra aprašomos trijų

dalelių Feinmano diagrama, buvo atlikti papildomi pakeitimai ir išplėtimai GRASP programos bibliotekoje „librang“, leidžiantys apskaičiuoti šios diagramos sukinines-kampines dalis. Darbe, kaip metodo taikymo pavyzdys, taip pat pateikiami Se III energijos struktūros skaičiavimai. Be to, išplėstasis metodas buvo pritaikytas atrinkti svarbiausias konfigūracinių būsenų funkcijas ir panaudoti jas suderintinio lauko lygtims spręsti.

* Skiriama akad. Zenono Rokaus Rudziko (1940–2011) gimimo sukakčiai paminėti.